Immune cell complexity in the tumor microenvironment of breast cancer

Salvagno, C.

CHAPTER 3

Transcriptional signatures derived from murine tumor-associated macrophages predict outcome in breast cancer patients

Sander Tuit[1,2,*], Camilla Salvagno[3,*], Theodore S. Kapellos[1,*], Cheei-Sing Hau[3], Lea Seep[1], Marie Oestereich[1], Kathrin Klee[1], Karin E. de Visser[3,#], Thomas Ulas[1,#] and Joachim L. Schultze[1,4,#]

[1] Genomics and Immunoregulation, LIMES Institute, University of Bonn, Carl-Troll-Str. 31, 53113 Bonn, Germany
[2] Department of Anatomy and Embryology, Leiden University Medical Center, Einthovenweg 20, 2333 ZC Leiden, The Netherlands
[3] Division of Tumor Biology & Immunology, Oncode Institute, the Netherlands Cancer Institute, Plesmanlaan 121, 1066 CX Amsterdam,The Netherlands
[4] Platform for Single Cell Genomics and Epigenomics (PRECISE) at the German Center for Neurodegenerative Diseases and the University of Bonn, Sigmund-Freud-Str. 27, 53127 Bonn, Germany
[*] shared first authorship
[#] shared last authorship

Corresponding authors: E-mail: j.schultze@uni-bonn.de, tel: (+49) 228 7362787;
E-mail: k.d.visser@nki.nl, tel: (+31) 20 5126104

Submitted for publication

Abstract

Tumor-associated macrophages (TAMs) are frequently the most abundant immune cells in murine and human cancers and are associated with poor survival. Here we generated TAM molecular signatures from K14cre;Cdh1flox/flox;Trp53flox/flox (KEP) and MMTV-NeuT (NeuT) transgenic mice which resemble human invasive lobular carcinoma (ILC) and HER2+ tumors, respectively. Determination of TAM-specific signatures in breast cancer required relationship analysis with healthy mammary tissue macrophages, since comparison with other macrophage populations overestimated TAM-specific gene expression. TAMs from the two models featured a distinct transcriptomic profile and KEP-derived signatures reliably predicted outcome in ILC patients, indicating that translation of murine TAM signatures to patients warrants consideration of the cancer subtype. Collectively, we show that a transgenic mouse tumor model can be utilized to derive a TAM signature for human breast cancer outcome prediction and we provide a generalizable strategy for determining and applying immune cell signatures provided the murine model reflects the human disease.

Introduction

The immune system plays an important role during tumor development, progression and therapy response and immune cells have evolved into attractive targets of therapeutic manipulation in cancer patients [1–3]. Ongoing and future attempts to fine-map the immune cell landscape of tumors will give us a full picture of the tumor microenvironment (TME) and may provide novel biomarkers and therapeutic targets [4]. Myeloid cells and, in particular, tumor-associated macrophages (TAMs) are a major component of the TME [5]. In the majority of cancer types, TAMs are often described as pro-tumorigenic and an enrichment of TAMs - as defined by immunohistochemistry and flow cytometry - has been linked to poor clinical outcome in several cancer types, including breast and lung cancers [6,7].

More recently, large multi-omics datasets from different cancer types consisting of thousands of human samples have been used to classify tumors based on immune cell-derived molecular signatures that could potentially be exploited in the future to improve patient stratification and therapeutic strategies [8–10]. For example, in colorectal cancer and T cell lymphomas, T cell-related gene signatures based on transcriptomic data were successfully used to diagnose, classify and predict disease outcome [11,12]. However, despite the enormous progress in the deconvolution of such data [13], the association of TAMs with clinically predictive signatures is not yet resolved.

Previous approaches to define might have been hampered by the fact that macrophages possess a tissue-specific transcriptional profile [14–16]. Consequently, the identification of TAM-specific signatures is not possible without access to healthy tissue macrophages of the same organ. Such reference data are still very limited [17] and efforts, such as the Human Cell Atlas[18] are not yet ready to provide such information. Whether or not the generation of cell type-specific signatures by single-cell transcriptomics [19–23] will be sufficient to infer TAM-specific signatures is currently not clear, considering the sparse nature of single-cell RNA-seq data.

In light of current shortcomings, we propose an alternative approach to define TAM-specific signatures and test their clinical applicability for outcome prediction. We first defined TAM signatures in well-defined murine tumor models by comparison with macrophages from different organs including the organ of tumor origin. For proof-of-principle, we generated TAM signatures from the K14cre;Cdh1flox/flox;Trp53flox/flox (KEP) murine breast cancer model [24] which recapitulates human ILC, the second most common histotype in humans, accounting for 10-15% of all breast cancers and the MMTV-NeuT (NeuT) breast cancer model[25] which has been indicated to resemble HER-2 positive breast cancers. Beside showing a shared transcriptional profile, TAMs from the two models present unique molecular signatures, illustrating the impact of the tumor subtype on TAMs. Tumor model-specific TAM signatures were then applied to clinical samples from large existing multi-omics studies[26,27] to assess the value of these TAM-specific signatures for predicting clinical outcome.

Results

Characterization of TAMs in two murine breast cancer models

We first characterized TAMs isolated from two spontaneous murine breast cancer models; the KEP (FVB background)[24] and the NeuT (Balb/c background) models [25] (Fig. 1a). Tumorigenesis in KEP mice is driven by the stochastic loss of E-cadherin and p53 by Keratin 14-specific Cre expression. These mice develop mammary tumors between 6-8 months of age and the disease resembles ILC in its pathology and progression [24]. In contrast, NeuT mice develop mammary tumors at 4 months of age due to the transgenic overexpression of the activated form of the rat oncogene *Neu* (ortholog of the human *HER2*) [25], previously indicated to resemble HER2^{+} breast tumors.

Assessment of the myeloid cell compartment in mammary tumors of both breast cancer models identified a CD11b^{hi}F4/80$^{low/-}$ population which contained Ly-6C^{hi} monocytes and Ly-6G^{hi}Ly-6C^{low} neutrophils and a CD11b^{hi}F4/80^{hi} macrophage population, hereafter referred to as TAMs (Fig. 1b-c). Next, we compared by immunohistochemistry the prevalence of macrophages in the mammary glands of age-matched WT mice, KEP and NeuT mice bearing early lesions and KEP and NeuT mice bearing tumors and found that both models were characterized by an increased accumulation of TAMs (Fig. 1d). Quantification of their numbers showed that CD11b^{hi}F4/80^{hi} macrophages represented 30% and 6% of the total live cells in the KEP and NeuT mammary tumors, respectively (Fig. 1e).

Further characterization of the macrophage phenotype showed that TAMs from the KEP and not from the NeuT model have lower expression of the mannose receptor CD206, while a higher proportion of TAMs in the NeuT model and not in the KEP model expresses higher levels of MHC-II compared to macrophages from the mammary gland of WT mice (Suppl. Fig. 1a-d). In addition, a significant increase in the frequency of Ki67^{+} TAMs was observed only in the KEP model compared to macrophages from healthy mammary glands of wild type FVB mice, (Suppl. Fig. 1e-f). Based on these data, we defined and sorted CD11b^{hi}F4/80^{hi} breast cancer TAMs, as well as tissue-resident macrophages from the mammary gland of KEP and NeuT mice (MTMs (KEP model), MTMs (NeuT model)), mammary tissue macrophages from KEP mice containing early neoplastic lesions, but not palpable tumors (MTMs (PRE-KEP model)) and spleen and bone marrow of WT and mammary tumor-bearing mice (WT spleen/BM (KEP/NeuT model) and spleen/BM (KEP/NeuT model)) for genome-wide assessment of transcriptional regulation (Suppl. Fig. 2a-h).

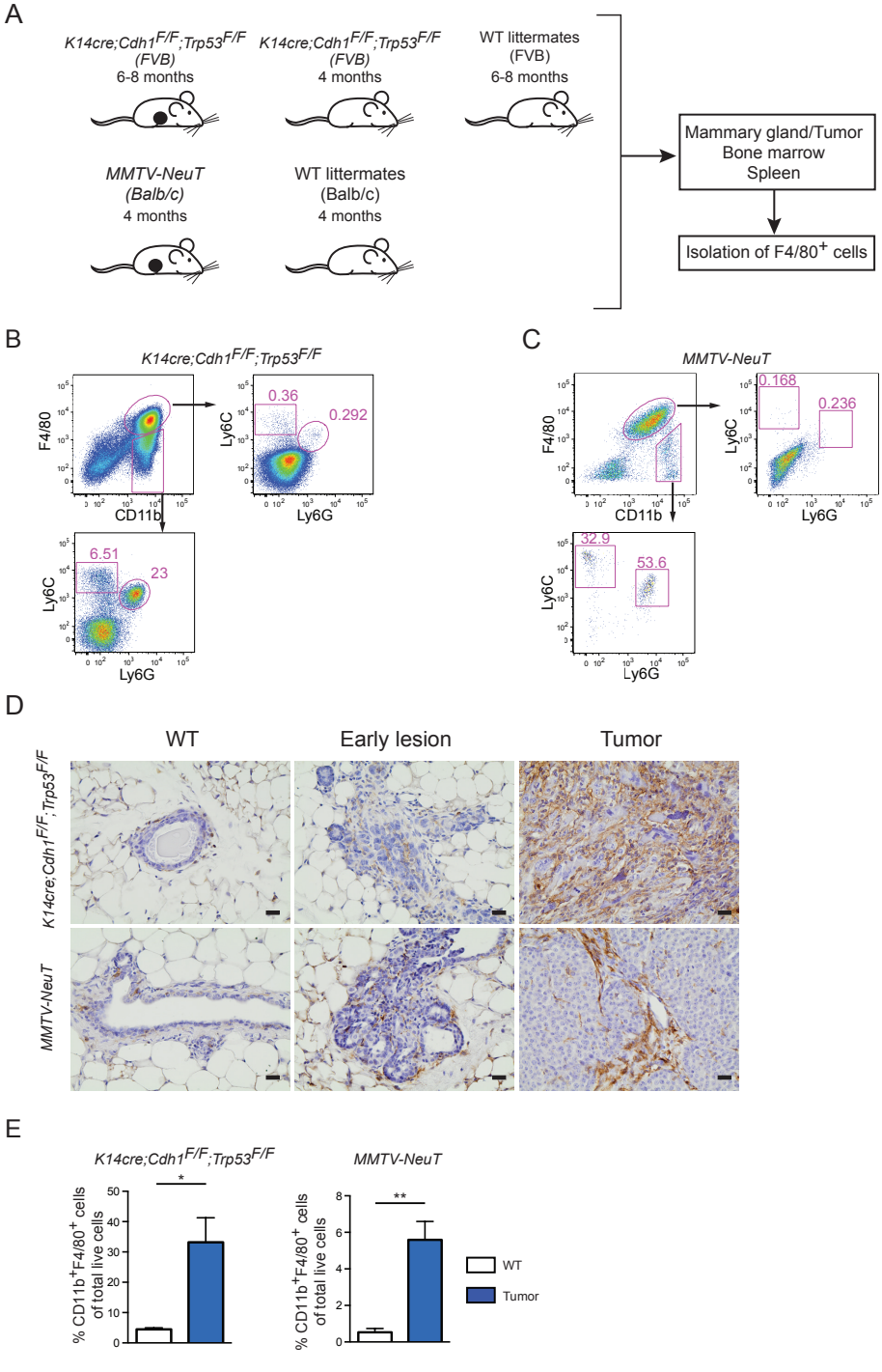
A
K14cre;Cdh1F/F;Trp53F/F (FVB) 6-8 months
K14cre;Cdh1F/F;Trp53F/F (FVB) 4 months
WT littermates (FVB) 6-8 months
MMTV-NeuT (Balb/c) 4 months
WT littermates (Balb/c) 4 months
Mammary gland/Tumor
Bone marrow
Spleen
Isolation of F4/80+ cells
B
K14cre;Cdh1F/F;Trp53F/F
F4/80
CD11b
Ly6C
Ly6G
0.36
0.292
6.51
23
C
MMTV-NeuT
0.168
0.236
32.9
53.6
D
WT
Early lesion
Tumor
K14cre;Cdh1F/F;Trp53F/F
MMTV-NeuT
E
K14cre;Cdh1F/F;Trp53F/F
MMTV-NeuT
% CD11b+F4/80+ cells of total live cells
WT
Tumor

Fig. 1 | Mammary tumorigenesis in two transgenic mouse models is characterized by macrophage influx. (a) Schematic representation of the macrophage sample collection for RNA sequencing. (b-c) Representative dot plots of a KEP mammary tumor (b) and a NeuT tumor (c) stained for F4/80 and CD11b, confirming absence of monocytes (Ly-6G$^-$Ly-6C$^+$) and neutrophils (Ly-6G$^+$Ly-6C^{low}) in the F4/80$^+$CD11b$^+$ TAM population. Dot plots are gated on CD45$^+$ cells. (d) Representative images of immunohistochemical F4/80 staining of a mammary gland from a WT FVB mouse, an early lesion in the mammary gland of a 4 months old KEP mouse and a KEP tumor (upper row); and of a mammary gland of a WT Balb/c mouse, an early lesion in the mammary gland of a 2 months old NeuT mouse and an NeuT mammary tumor (lower row), scale bar= 20 um. (e) Average percentage of CD11b$^+$ F4/80$^+$ macrophages gated on live cells in mammary glands and mammary tumors of KEP mice (left graph) and in mammary glands and mammary tumors of NeuT mice (right graph). Data are mean ± SEM from n=5-6 animals per group and were analyzed with a Mann-Whitney test, *$p < 0.05$, **$p < 0.001$.

Tissue origin dictates transcriptional regulation of TAMs

Considering findings demonstrating that tissue macrophages are characterized by organ-specific transcriptional regulation [16], we first compared the transcriptome profiles of the TAMs derived from the two breast cancer models (KEP, NeuT) with publicly available TAM profiles of two lung cancer models (Lewis lung carcinoma cell line and lung adenocarcinoma cell line) and with the profiles of tissue-resident macrophages of the mammary gland or lung, respectively. In addition, macrophages harvested from seven organs derived from either WT, mammary tumor-bearing or helminth-infected mice as well as other immune and epithelial cells [16,28–31] were used as controls (Fig. 2a and Suppl. Fig. 3a-b). Cells of the macrophage/monocyte lineage clustered together, separated from T cells, neutrophils, NK cells and epithelial cells (Suppl. Fig. 3c).

To elaborate the relationship between the different tissue-resident macrophages and cancer models, we performed sample-sample co-expression network analysis (CNA) based on Pearson correlation (cutoff 0.977) on all present genes. CNA showed a distinct cluster consisting of mammary gland tissue macrophages (MTMs) and TAMs derived from both breast cancer models, strongly suggesting that the tissue of origin dictates most of the transcriptional regulation in TAMs (Fig. 2b). This was similarly true for the lung cancer TAMs isolated from the two cancer cell line-based models which clustered together with the healthy lung-derived macrophages. To computationally validate these findings, we performed hierarchical clustering (HC) on the 1,000 genes with the highest variance within the dataset (Fig. 2c) and generated a Pearson correlation coefficient matrix (PCCM) (Fig. 2d). Both approaches supported our initial findings, clearly indicating that the TAMs of the two breast cancer models and the two lung cancer models were part of the mammary gland or lung clusters, respectively. Similarly, macrophages derived from spleen or bone marrow of tumor-bearing KEP or NeuT mice also clustered with the respective organ (Fig. 2c-d). Moreover, we observed that the transcriptional differences between TAMs and their respective healthy tissue counterparts were less pronounced than those between healthy and helminth-infected animals (Fig. 2c-d).

As an alternative to statistical models, we employed CNA on all genes and created a scale-free network (R^2= 0.772) based on a Pearson correlation cutoff of 0.87 (Suppl. Fig. 4a-b). A total of 28 clusters were identified in the Co-expression Network Analysis (CoCena[2]) cluster-condition heatmap (Fig. 2e) and specific gene signatures for each of the macrophage samples were discovered in this network as depicted in Suppl. Fig. 4c. We detected modules associated with classic macrophage functions,

such as scavenger receptors (*Cd163*, *Mrc1*, *Cd36*) and transcription factors (*Maf*) in MTMs, whereas we identified genes, such as the pro-inflammatory *Il12b*, the integrin *Itgb8* and the G protein-coupled receptor *Gpr31b* mainly associated with breast cancer TAMs (Fig. 2f). Taken together, our data suggest that the tissue of origin dictates not only the transcriptomes of healthy tissue-resident macrophages, but also of TAMs and dictates their transcriptional programs.

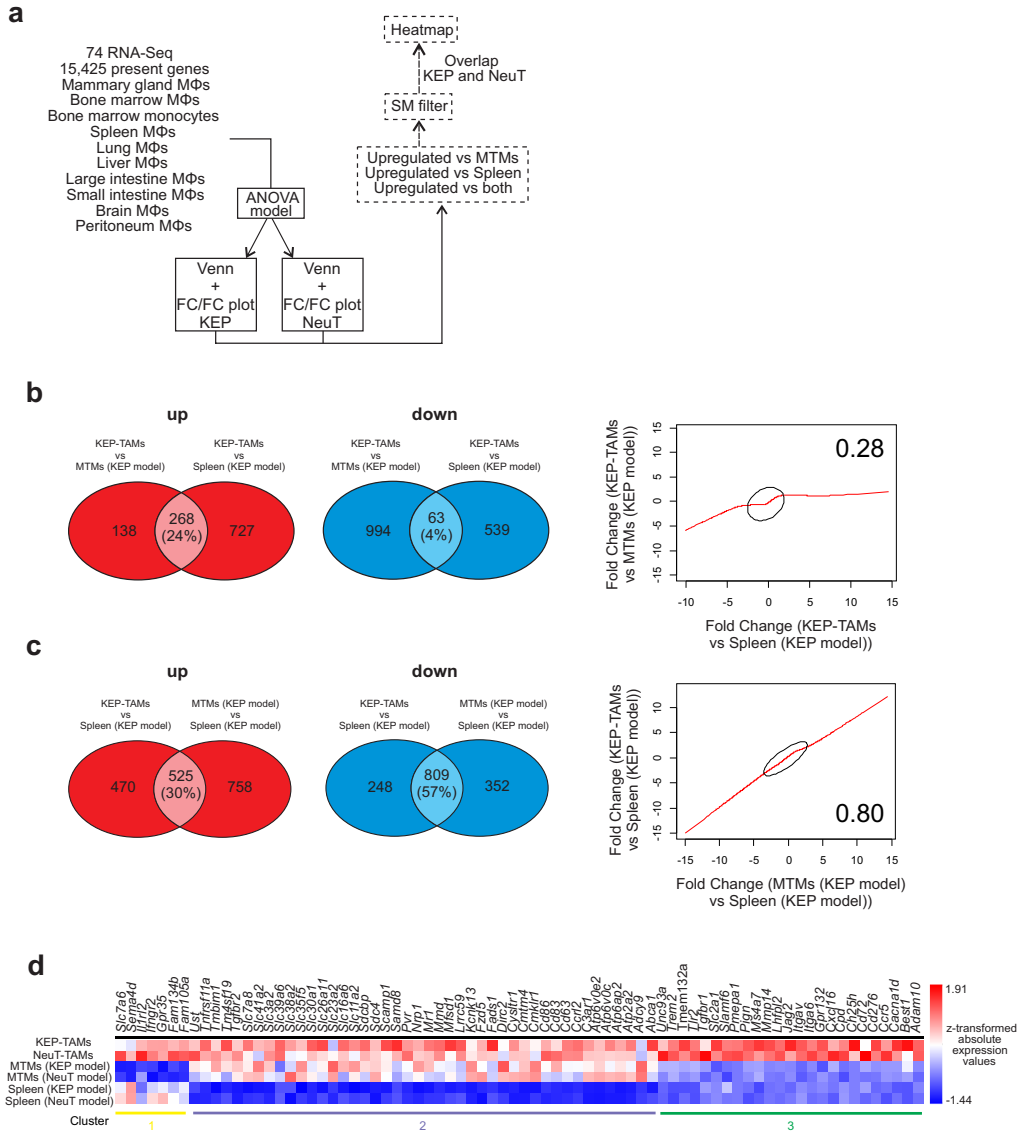

Fig. 2 | Tissue of origin determines the fate of the macrophage phenotype. (a) Schematic representation depicting the bioinformatics workflow. (b) Network visualization of sample-centered correlation analysis where each node represents one sample. (c-d) HC and PCCM maps based on the 1,000 genes with the highest variance within the dataset. Indicated in bold (d) are the disease state macrophages. (e) CoCena[2] cluster-condition heatmap and (f) CoCena[2] visualization of all present co-expressed genes in all tissues. Tissue-specific clusters for mammary gland/tumors are colored according to the clustering as seen in cluster-condition heatmap. Representative cluster-specific genes are noted next to them, GFC; Group Fold Change.

Identification of TAM-specific transcripts

Although the comparison of TAMs with different tissue-resident macrophage populations revealed that the tissue of origin is the major driver of the global transcriptome in TAMs, we were also interested to determine truly TAM-specific gene expression profiles. In previous reports, TAM functionalities have been compared to macrophages isolated from a different tissue than the tumor origin[32,33]. We, in contrast, defined such genes by direct comparison of breast cancer TAMs with macrophages from age-matched healthy mammary gland tissue and related them to those derived from comparisons of TAMs with other tissue-resident macrophages (Fig. 3). We employed Venn diagrams to compare KEP-TAMs with either MTMs or splenic macrophages (KEP model) (Fig. 3b), as well as splenic macrophages (KEP model) with either KEP-TAMs or MTMs (KEP model) (Fig. 3c). We found that the fold change of differentially expressed (DE) genes in the TAMs versus splenic macrophages correlated better with the fold change of DE genes in the MTMs versus splenic macrophages (KEP model) (r=0.8) as opposed to the fold change of DE genes in the TAMs versus MTMs (KEP model) (r=0.28), indicating an overestimation of differential gene expression by TAMs when comparing to splenic macrophages (Fig. 3b-c). This was also reflected in the respective FC/FC plots where many genes were similarly DE when plotting KEP-TAMs versus either MTMs (KEP model) or splenic macrophages (Suppl. Fig. 5a). Plotting KEP-TAMs versus splenic macrophages against MTMs indicated that the TAMs and MTMs displayed a transcriptome profile substantially different from that of splenic macrophages (Suppl. Fig. 5b). Similarly, the same pattern was observed in the NeuT model (Suppl. Fig. 5c-d) or when splenic macrophages were replaced with bone marrow macrophages in both breast cancer models (Suppl. Fig. 5e-h).

To identify truly TAM-associated cell surface markers, we plotted genes elevated in TAMs in comparison to either MTMs or splenic macrophages from both models (Fig. 3d). This analysis revealed a small set of genes that was DE against both MTMs and splenic macrophages (cluster 3). Moreover, we also identified genes which were DE only against splenic macrophages (cluster 2) or MTMs (cluster 1) and which would wrongfully be included or excluded from downstream analysis if splenic macrophages were to be used as the reference macrophage population. Collectively, these analyses further support the notion that the determination of TAM transcriptomic profiles requires comparison to macrophages derived from the same tissue and strongly argue for the careful selection of reference macrophage populations.

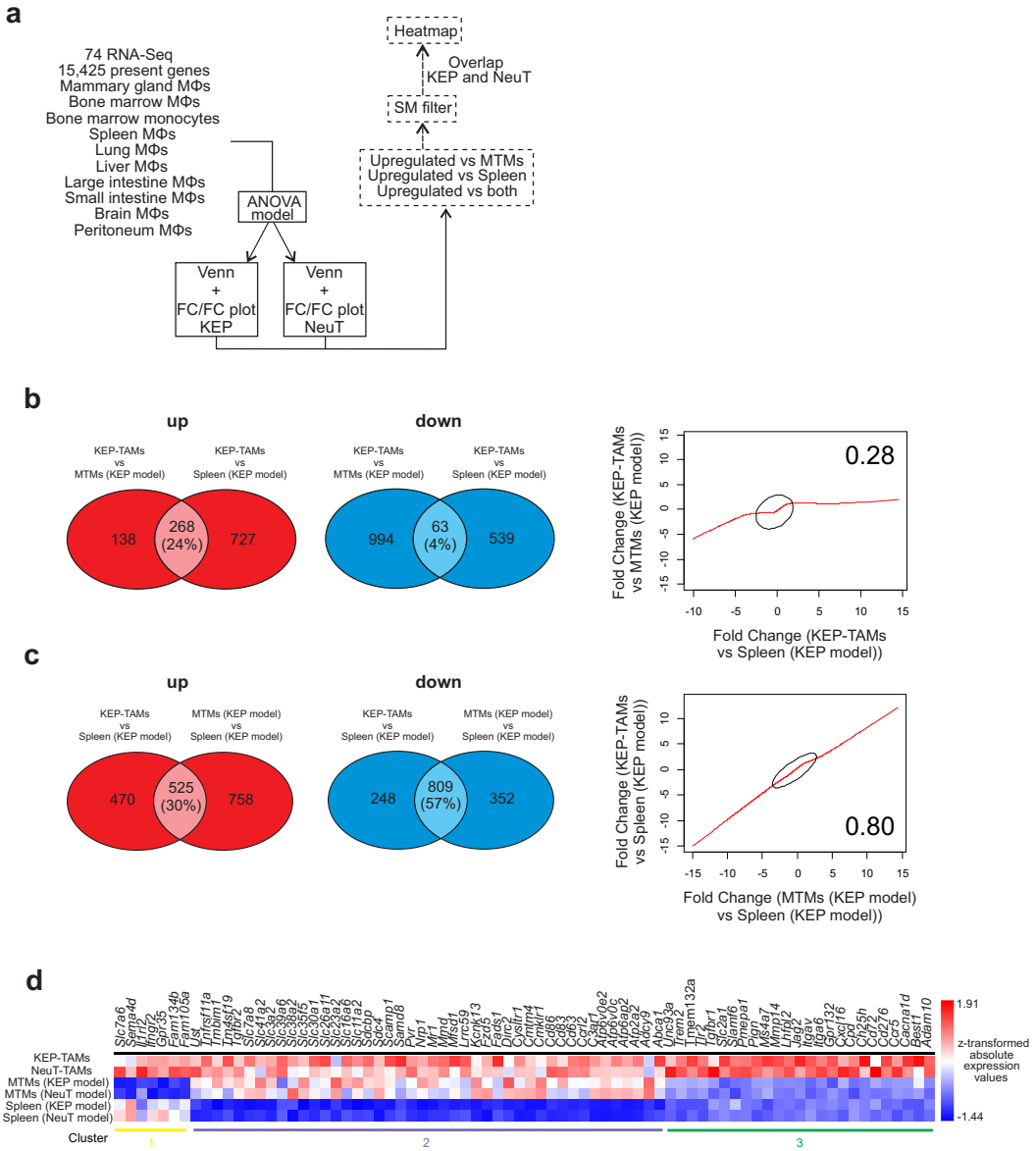

Fig. 3 | Inter-tissue comparison leads to false interpretation of changes in TAMs. (a) Schematic representation outlining the bioinformatics approach. (b-c) Venn diagrams of the comparisons of KEP-TAMs with MTMs and splenic macrophages (KEP model) (b) and splenic macrophages with KEP-TAMs and MTMs (KEP model) (c). Correlation plots of the fold changes of the DE genes in the aforementioned comparisons are shown (right) for both Venn diagrams. (d) Heatmap visualization of z-transformed surface marker (SM) absolute expression values. Overlapping DE genes from KEP and NeuT models were extracted from FC/FC plots, filtered for SMs and plotted.

TAM transcriptomes differ between different breast cancer models

Our experimental setting also allowed us to define tumor model-specific regulation of macrophages (Fig. 4a). To define differences in TAM transcriptomes between the KEP and the NeuT model, we performed principal component analysis (PCA) (Fig. 4b), HC of the 1,000 genes with the highest variance (Fig. 4c) and PCCM (Fig. 4d). All three approaches demonstrated that TAMs from both breast cancer models are more closely related to each other than to MTMs from healthy or early neoplastic lesions. However, we also identified tumor model-specific gene alterations in TAMs as depicted in the HC analysis of KEP and NeuT models (Fig. 4c, clusters 5 and 8, respectively), implying that the tumor subtype also shapes the transcriptional regulation of TAMs. Two clusters (1 and 4) are related to the different genetic backgrounds of the models as the same up or downregulated genes in KEP-TAMs and NeuT-TAMs were also seen in MTMs (KEP model) and MTMs (NeuT model),respectively. Representative genes from clusters 5 (*Hif1a*, *Vegfa*, *Itgam*, *Cxcr4*, *Il1rn*) and 8 (*Tlr12*, *Itga8*, *Itgb8*, *Icosl*) of the HC are depicted in the model-specific Volcano plots of Fig. 4e-f.

We next visualized the DE genes from the comparison of KEP-TAMs and NeuT-TAMs to the respective MTMs in Venn diagrams to determine the overlap between the two models and found a small overlap in both the upregulated (17%, upper diagram) and downregulated (26%, lower diagram) DE genes (Fig. 4g). Since we also had the opportunity to isolate MTMs (PRE-KEP model), we could determine whether there were already transcriptional changes in macrophages at this stage. However, the transcriptional changes of MTMs (PRE-KEP model) to KEP-TAMs were comparable to those of healthy MTMs to KEP-TAMs as shown in the respective Venn diagrams for upregulated (70%, upper diagram) and downregulated (50%, lower diagram) DE genes, suggesting that they are similar to each other (Fig. 4h).

Based on the DE genes in both tumor models, we inferred overall biological changes by gene ontology enrichment analysis (GOEA) (Suppl. Fig. 6a-c). Common breast cancer TAM ontology terms included proliferation-related processes, regulation of innate immune responses and cell migration properties, wound healing processes and T cell activation processes (Suppl. Fig. 6a), whereas vasculature development and cell cycle-related processes (KEP-TAMs) and regulation of cell growth and angiogenesis-related processes (NeuT-TAMs) were associated with model-specific TAM populations (Suppl. Fig. 6b-c). Notably, the cell cycle-related processes were only significantly enriched in KEP-TAMs which is in line with the phenotypical observations of Suppl. Fig. 1e-f. In conclusion, our data show that the breast cancer subtype contributes to TAM transcriptional differences in different murine models.

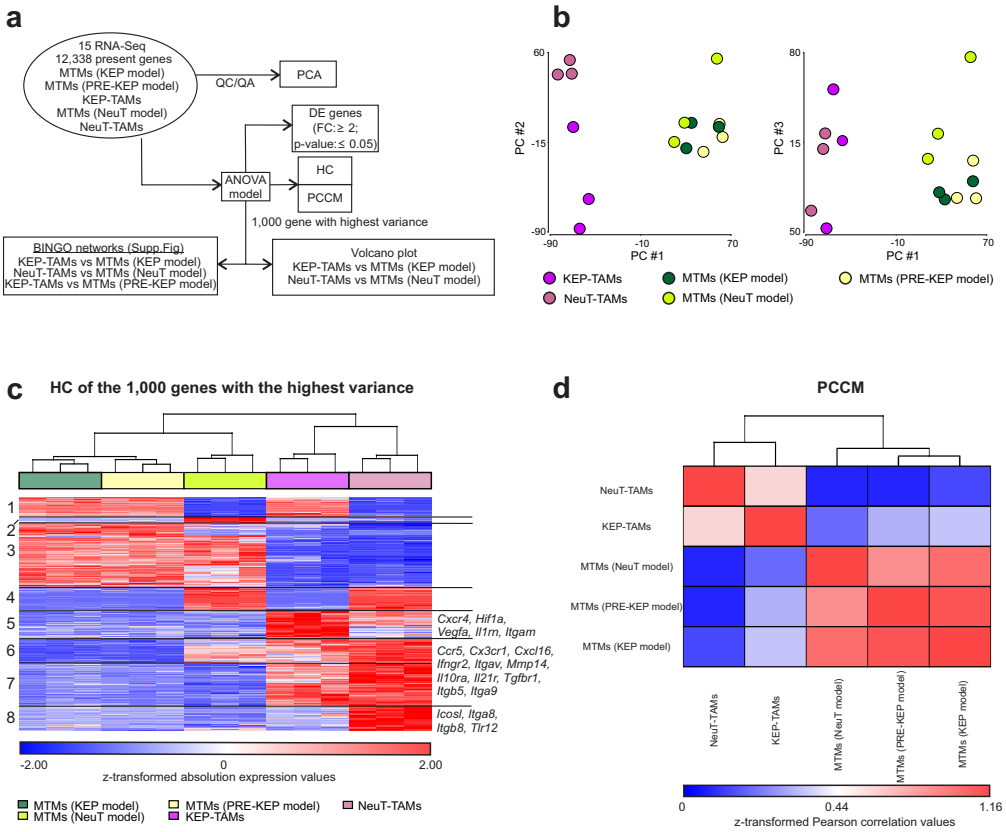
a
15 RNA-Seq
12,338 present genes
MTMs (KEP model)
MTMs (PRE-KEP model)
KEP-TAMs
MTMs (NeuT model)
NeuT-TAMs
QC/QA
PCA
DE genes
(FC:≥ 2;
p-value:≤ 0.05)
ANOVA
model
HC
PCCM
1,000 gene with highest variance
BINGO networks (Supp.Fig)
KEP-TAMs vs MTMs (KEP model)
NeuT-TAMs vs MTMs (NeuT model)
KEP-TAMs vs MTMs (PRE-KEP model)
Volcano plot
KEP-TAMs vs MTMs (KEP model)
NeuT-TAMs vs MTMs (NeuT model)
b
PC #2
PC #1
PC #3
PC #1
KEP-TAMs
MTMs (KEP model)
MTMs (PRE-KEP model)
NeuT-TAMs
MTMs (NeuT model)
c
HC of the 1,000 genes with the highest variance
Cxcr4, Hif1a, Vegfa, Il1rn, Itgam
Ccr5, Cx3cr1, Cxcl16, Ifngr2, Itgav, Mmp14, Il10ra, Il21r, Tgfbr1, Itgb5, Itga9
Icosl, Itga8, Itgb8, Tlr12
z-transformed absolution expression values
MTMs (KEP model)
MTMs (NeuT model)
MTMs (PRE-KEP model)
KEP-TAMs
NeuT-TAMs
d
PCCM
NeuT-TAMs
KEP-TAMs
MTMs (NeuT model)
MTMs (PRE-KEP model)
MTMs (KEP model)
z-transformed Pearson correlation values

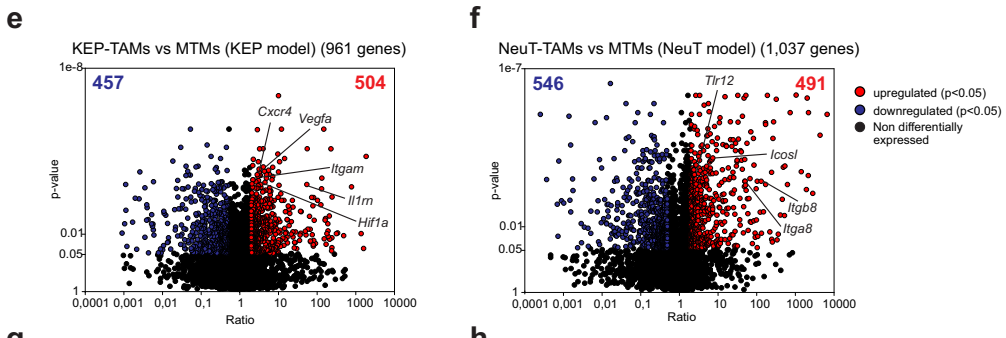
e
KEP-TAMs vs MTMs (KEP model) (961 genes)
457
504
Cxcr4
Vegfa
Itgam
Il1rn
Hif1a
p-value
Ratio
f
NeuT-TAMs vs MTMs (NeuT model) (1,037 genes)
546
491
Tlr12
Icosl
Itgb8
Itga8
upregulated (p<0.05)
downregulated (p<0.05)
Non differentially expressed

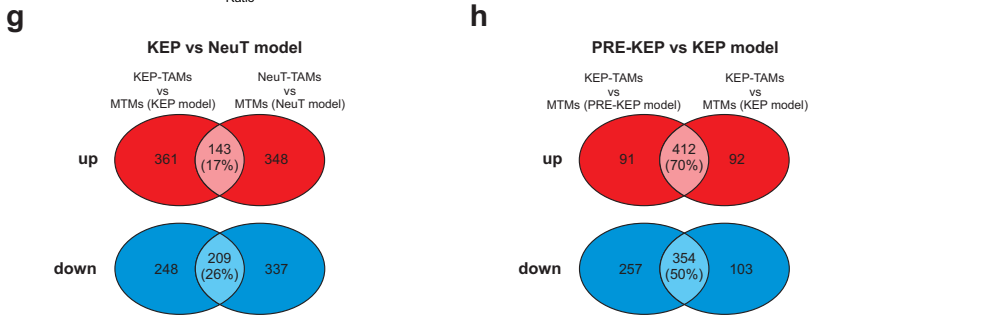
g
KEP vs NeuT model
KEP-TAMs vs MTMs (KEP model)
NeuT-TAMs vs MTMs (NeuT model)
up
361
143 (17%)
348
down
248
209 (26%)
337
h
PRE-KEP vs KEP model
KEP-TAMs vs MTMs (PRE-KEP model)
KEP-TAMs vs MTMs (KEP model)
up
91
412 (70%)
92
down
257
354 (50%)
103

Fig. 4 | Breast cancer subtype influences TAM phenotype - conventional approach. (a) Schematic representation outlining the bioinformatics approach. (b) PCA using all present (12338) genes with principle components (PC1-2 and PC1-3) plotted in two-dimensional graphs. (c) HC map based on the 1,000 genes with the highest variance within the dataset.
Representative cluster-specific genes are noted next to them. (d) PCCM map based on the 1,000 genes with the highest variance within the dataset. (e) Volcano plot of the DE genes from the comparison KEP-TAMs with MTMs (KEP model). (f) Volcano plot of the DE genes from the comparison NeuT-TAMs with MTMs (NeuT model). DE genes (FC ≥ 2, FDR-adjusted p-value ≤ 0.05) are indicated in red and representative upregulated DE genes are noted. (g) Venn diagram of the comparisons of KEP-TAMs with MTMs (KEP model) and NeuT-TAMs with MTMs (NeuT model). (h) Venn diagram of the comparisons of KEP-TAMs with MTMs (PRE-KEP model) and KEP-TAMs with MTMs (KEP model).

Identification of TAM-associated hubs by CNA

To link our information concerning differential transcriptional regulation within TAMs of different models to potential regulatory circuits, we utilized co-regulation of gene expression as our model and applied CNA on the DE genes between TAMs and MTMs in at least one of the breast cancer models (Fig. 5). The scale-free network (Fig. 5b, R^2=0.714) comprised 8 modules and confirmed that the transcriptomes of KEP-TAMs and NeuT-TAMs consisted of genes which followed shared (turquoise module) and model-specific expression patterns (blue and magenta modules) (Fig. 5c). Immune-related DE genes which were co-expressed are shown for the turquoise (*Ccr5*, *Cx3cr1*, *Cxcl16*, *Ifngr2*, *Itgav*, *Mmp14*), blue (*Cxcr4*, *Hif1a*, *Itgam*) and magenta (*Icosl*, *Itga8*, *Itgb8*, *Tlr12*) modules in Fig. 5d.
We then went one step further and investigated the potential hierarchies in TAM-associated gene regulation by building Intraclusteral Gene Interaction Networks (I-GINs) which extend the network approach. From the previous network analysis, we first focused on the gene module changed in both TAM models (turquoise module). We visualized the top 25% nodes based on degree and correlation and the top 25% correlation-ranked edges to identify known interactions from the STRING protein-protein interactions database (Fig. 5e). Subsequently, all edges to hubs were kept allowing a maximum of two edges between hubs. Already 46% of the identified interactions within the common breast cancer TAM network were known based on protein-protein interaction databases. Among the selected candidates, we detected cytokine receptors (*Ifngr2*), chemokines (*Cxcl16*) and metalloproteinases (*Mmp14*) which reflect the immune activation of breast cancer TAMs in the TME (Fig. 5f). Further assessment of the KEP-TAM- and NeuT-TAM-specific modules revealed the co-regulation of hypoxia factor (*Hif1a*) and scavenger receptors (*Msr1*) in the KEP-TAM dataset and pathogen recognition receptors (*Tlr12*), co-stimulatory molecules (*Icosl*) and integrins (*Itgax*) in the NeuT-TAM dataset (Suppl. Fig. 7). Finally, the co-expressed genes detected here presented a remarkably high degree of overlap with the DE genes identified by statistical models in Fig. 4c, further strengthening their relevance as breast cancer model-specific biomarkers in TAMs.

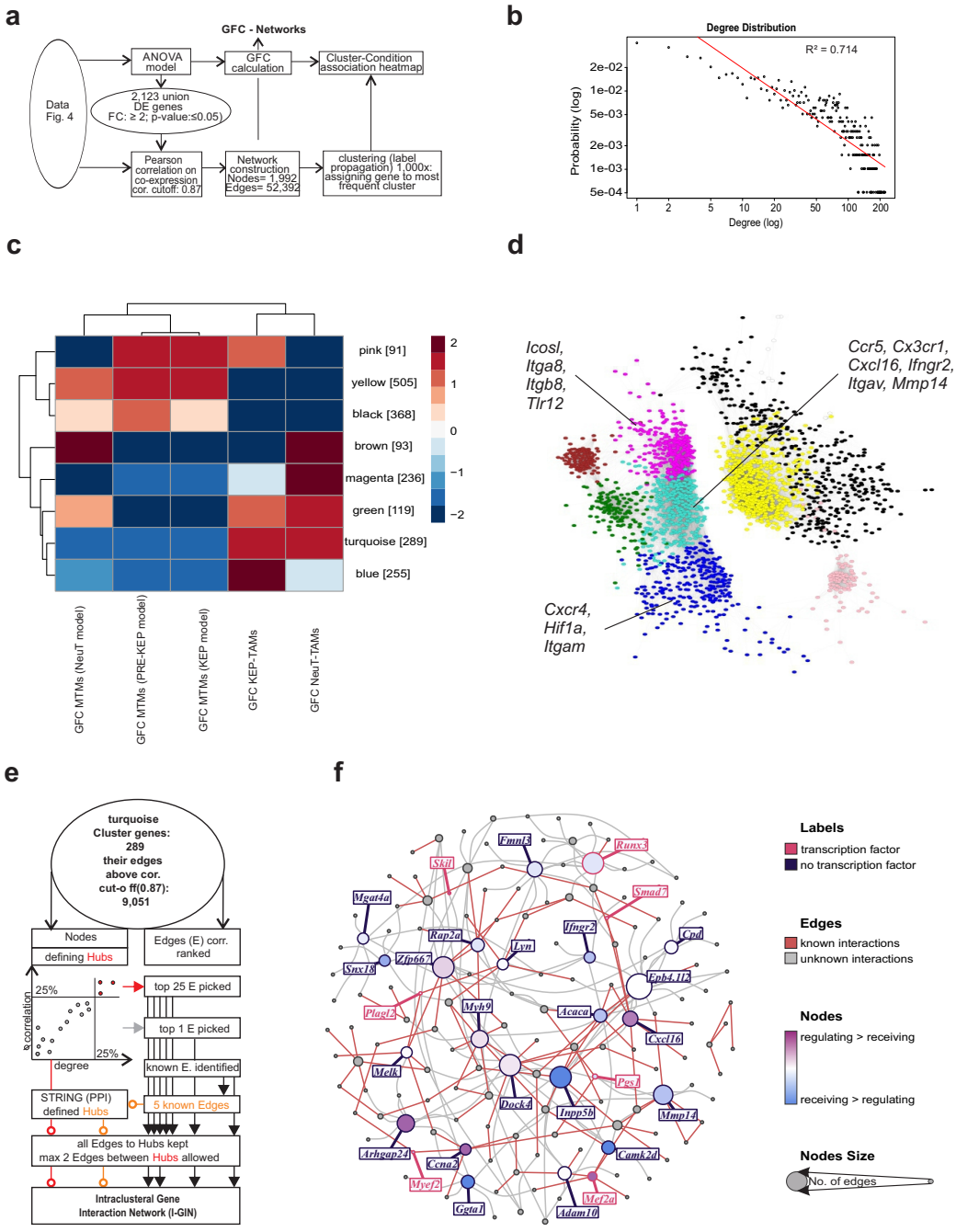
a
GFC - Networks
Data
Fig. 4
ANOVA
model
GFC
calculation
Cluster-Condition
association heatmap
2,123 union
DE genes
FC: ≥ 2; p-value:≤0.05)
Pearson
correlation on
co-expression
cor. cutoff: 0.87
Network
construction
Nodes= 1,992
Edges= 52,392
clustering (label
propagation) 1,000x:
assigning gene to most
frequent cluster
b
Degree Distribution
R² = 0.714
Probability (log)
2e-02
1e-02
5e-03
2e-03
1e-03
5e-04
1
2
5
10
20
50
100
200
Degree (log)
c
pink [91]
yellow [505]
black [368]
brown [93]
magenta [236]
green [119]
turquoise [289]
blue [255]
2
1
0
−1
−2
GFC MTMs (NeuT model)
GFC MTMs (PRE-KEP model)
GFC MTMs (KEP model)
GFC KEP-TAMs
GFC NeuT-TAMs
d
Icosl,
Itga8,
Itgb8,
Tlr12
Ccr5, Cx3cr1,
Cxcl16, Ifngr2,
Itgav, Mmp14
Cxcr4,
Hif1a,
Itgam
e
turquoise
Cluster genes:
289
their edges
above cor.
cut-o ff(0.87):
9,051
Nodes
defining Hubs
Edges (E) corr.
ranked
25%
top 25 E picked
top 1 E picked
25%
degree
known E. identified
STRING (PPI)
defined Hubs
5 known Edges
all Edges to Hubs kept
max 2 Edges between Hubs allowed
Intraclusteral Gene
Interaction Network (I-GIN)
f
Fmnl3
Runx3
Skil
Mgat4a
Smad7
Rap2a
Ifngr2
Cpd
Lyn
Snx18
Zfp667
Epb4.1l2
Plagl2
Myh9
Acaca
Cxcl16
Melk
Pex1
Dock4
Inpp5b
Mmp14
Arhgap24
Ccna2
Camk2d
Myef2
Mef2a
Ggta1
Adam10
Labels
transcription factor
no transcription factor
Edges
known interactions
unknown interactions
Nodes
regulating > receiving
receiving > regulating
Nodes Size
No. of edges

Fig. 5 |Breast cancer subtype influences TAM phenotype - co-expression-based approach. (a) Schematic representation outlining bioinformatics workflow. (b) CoCena[2] logged network degree distribution with linear fitting. (c) CoCena[2] cluster-condition heatmap. (d) CoCena[2] visualization of all present co-expressed genes. Network nodes are colored according to their cluster membership and representative cluster-specific genes are noted. (e) Schematic representation outlining bioinformatics workflow for I-GIN construction for breast cancer TAM-specific genes (turquoise cluster). (f) I-GIN node coloring represents regulatory or receiving status obtained from a Bayesian approach and points out highly co-expressed genes and their known or proposed links to strongest correlated neighbors. Candidate genes mentioned in the text are highlighted in yellow boxes. GFC; Group Fold Change

Model-specific TAM gene signatures predict disease outcome in humans

To determine the clinical relevance of the identified murine model-specific TAM signatures, we next set out to translate our findings to humans. For this purpose, we generated a unique list of TAM-associated genes defined by statistical and co-expression models (Fig. 6a), identifying 198 KEP-TAM associated genes, 227 NeuT-associated genes and 116 common breast cancer TAM genes (Fig. 6b). As a next step, we interrogated RNA-seq samples derived from ILC patients within the TCGA (n=125) [26] and the METABRIC (n=147) [27] databases for their macrophage content (Fig. 6c and Suppl. Fig. 8a). We used linear support vector regression (LSVR) and the LM22 macrophage gene signature set [34] to describe the immune cell content of these samples. When ranking the samples for predicted macrophage content, it became clear that ILC patients have quite variable amounts of macrophages within their tumor microenvironment (Fig. 6c). We also tested whether the specific murine TAM signatures could be identified (Suppl. Fig. 8a). Indeed, when applying LSVR using signatures derived from KEP-TAMs, NeuT-TAMs and respective MTMs, the KEP-TAM signatures represented a major part in most of the ILC patients (TCGA cohort), while the NeuT-TAM signatures were present to a lower extent in most of the cases (Suppl. Fig. 8a), indicating that the murine KEP-TAM signatures might better reflect the biology of TAMs in ILC patients.

Based on these encouraging results, we assessed the predictive value of these breast cancer model-specific TAM signatures for disease outcome. Kaplan-Meier analysis showed that the KEP-TAM signatures correlated with worse clinical outcome (p=0.037) of ILC patients from the TCGA cohort (Fig. 6d) and the METABRIC cohort (p=0.048) (Suppl. Fig. 8b). Importantly, the NeuT-TAM signatures were not enriched in ILC patients or did not correlate with better or worse overall survival in both patient cohorts (Fig. 6e and Suppl. Fig. 8c). To further prove the validity of these findings, we used gene signatures from the comparison of KEP-TAMs with splenic macrophages, random signatures and LSVR-derived total human macrophage signatures and assessed whether they were predictive of the outcome in the TCGA and METABRIC ILC cohorts (Fig. 6f-g, Suppl. Fig. 8d-g). In fact, none of these signatures showed a predictive value of disease outcome of ILC patients (separation of Kaplan-Meier groups or gene signature enrichment z score) in both cohorts. Collectively, these data indicate that the generation of meaningful gene signatures for outcome prediction derived from TAMs requires a clinically relevant murine model (here the KEP model for ILC) and the comparison of TAMs with their healthy tissue counterparts -here MTMs- instead of unrelated macrophage sources such as spleen or bone marrow.

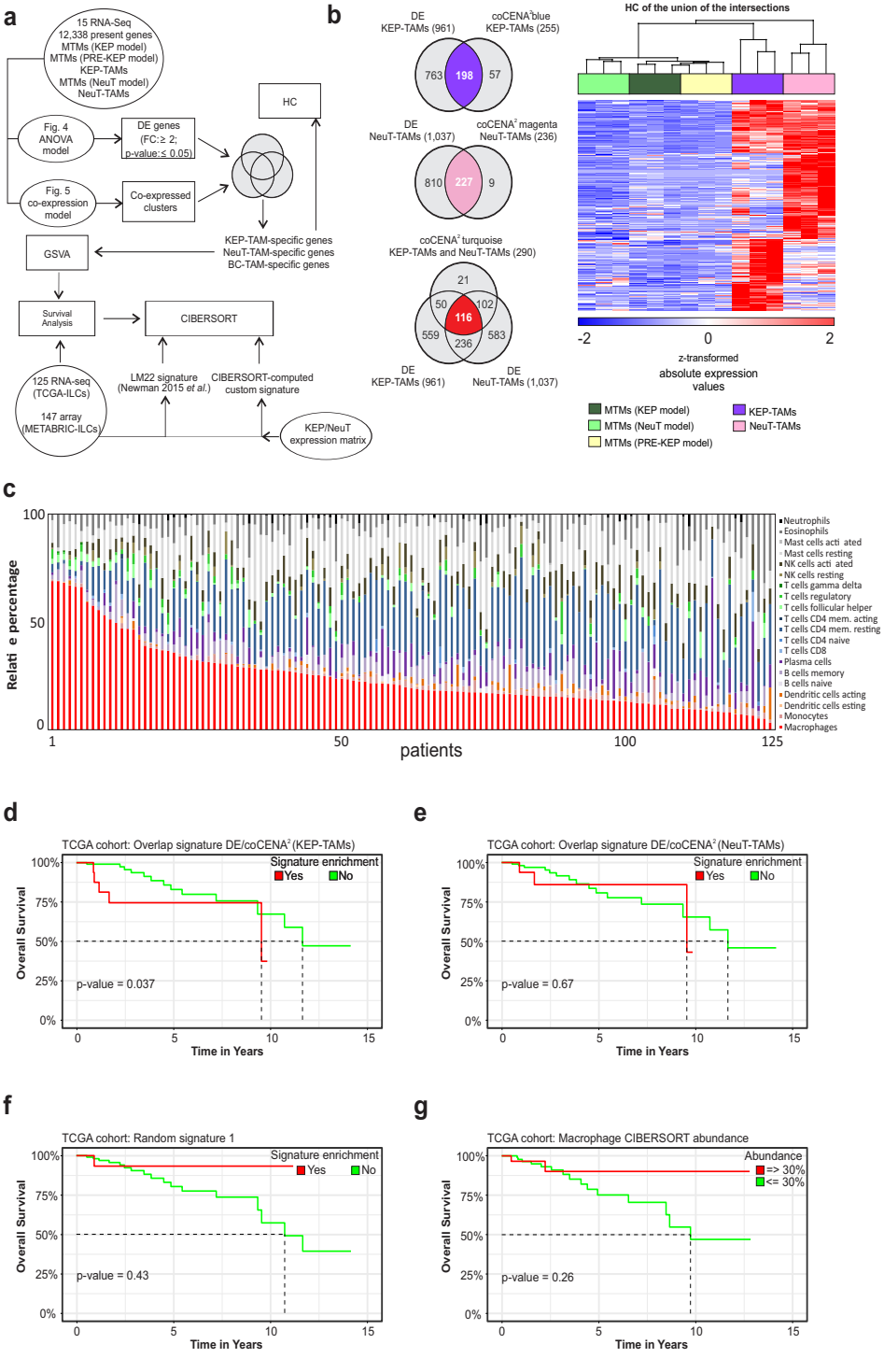
a
15 RNA-Seq
12,338 present genes
MTMs (KEP model)
MTMs (PRE-KEP model)
KEP-TAMs
MTMs (NeuT model)
NeuT-TAMs
Fig. 4 ANOVA model
DE genes (FC:≥ 2; p-value:≤ 0.05)
Fig. 5 co-expression model
Co-expressed clusters
HC
KEP-TAM-specific genes
NeuT-TAM-specific genes
BC-TAM-specific genes
GSVA
Survival Analysis
CIBERSORT
125 RNA-seq (TCGA-ILCs)
147 array (METABRIC-ILCs)
LM22 signature (Newman 2015 et al.)
CIBERSORT-computed custom signature
KEP/NeuT expression matrix
b
DE KEP-TAMs (961)
coCENA2blue KEP-TAMs (255)
763
198
57
DE NeuT-TAMs (1,037)
coCENA2 magenta NeuT-TAMs (236)
810
227
9
coCENA2 turquoise KEP-TAMs and NeuT-TAMs (290)
21
50
102
116
559
236
583
DE KEP-TAMs (961)
DE NeuT-TAMs (1,037)
HC of the union of the intersections
-2
0
2
z-transformed
absolute expression values
MTMs (KEP model)
MTMs (NeuT model)
MTMs (PRE-KEP model)
KEP-TAMs
NeuT-TAMs
c
Relati e percentage
100
50
0
1
50
100
125
patients
Neutrophils
Eosinophils
Mast cells acti ated
Mast cells resting
NK cells acti ated
NK cells resting
T cells gamma delta
T cells regulatory
T cells follicular helper
T cells CD4 mem. acting
T cells CD4 mem. resting
T cells CD4 naive
T cells CD8
Plasma cells
B cells memory
B cells naive
Dendritic cells acting
Dendritic cells esting
Monocytes
Macrophages
d
TCGA cohort: Overlap signature DE/coCENA2 (KEP-TAMs)
Signature enrichment
Yes
No
Overall Survival
100%
75%
50%
25%
0%
p-value = 0.037
0
5
10
15
Time in Years
e
TCGA cohort: Overlap signature DE/coCENA2 (NeuT-TAMs)
Signature enrichment
Yes
No
Overall Survival
p-value = 0.67
Time in Years
f
TCGA cohort: Random signature 1
Signature enrichment
Yes
No
Overall Survival
p-value = 0.43
Time in Years
g
TCGA cohort: Macrophage CIBERSORT abundance
Abundance
=> 30%
<= 30%
Overall Survival
p-value = 0.26
Time in Years

Fig. 6 | KEP-TAM-specific signatures predict overall survival in ILC patients. (a) Schematic representation depicting the bioinformatics approach. (b) Venn diagrams of overlapping CoCena[2]- and ANOVA-derived gene sets for KEP-TAMs (up), NeuT-TAMs (middle) and breast cancer TAMs (bottom) (left), HC map of the union of KEP-TAM-, NeuT-TAM- and breast cancer TAM-specific genes (right). (c) The "LM22" signatures (Newman et al. 2015) were used as input to identify the relative fraction of several immune cell populations in the ILC specimens (TCGA cohort, n=125). (d-g) Kaplan-Meier survival analysis of TCGA ILC patients. ILC specimens having a significant enrichment for KEP-TAMs signature (d), NeuT-TAMs signature (e), random signature (f) and CIBERSORT macrophage signature (g) are visualized in red line and numbers. The rest of ILC patients are visualized in green line and numbers. Z score above 2 marks significant enrichment of gene signatures.

Discussion

It is widely acknowledged that the immune system plays an important role in cancer development and progression [2]. Macrophages are one of the major components within the TME [35] and accumulating evidence indicates that their abundance is linked to disease outcome [36]. Here we provide a strategy to derive TAM-specific gene signatures and demonstrate that signatures derived from a transgenic murine tumor model for ILC can be used to predict outcome in two independent ILC cohorts (TCGA, METABRIC). These signatures could only be generated by proper comparison with the healthy tissue-resident macrophage counterparts, here MTMs, but not by comparison with macrophages derived from unrelated tissues, e.g. spleen or bone marrow. Moreover, we show that the global transcriptome of TAMs is mainly defined by tissue signals, although the tumor subtype also plays a crucial role in shaping the TAM transcriptional networks. Collectively, our approach illustrates how transcriptional regulation of TAMs derived from a murine model closely resembling the human disease (here ILC) [24] can be successfully translated into clinically meaningful disease outcome prediction.

Previous studies have defined TAM gene signatures by comparing TAMs to healthy tissue macrophages derived from tissues, such as the spleen [32,33]. However, recent evidence highlighted the diversity of the transcriptomes and epigenomes of the several tissue-resident macrophage populations [14,16]. With these findings at hand, it was conceivable to address whether such definitions would indeed lead to TAM-specific signatures. We provide compelling evidence that TAMs still share most genes with their healthy tissue counterparts both in breast and lung and that the comparison of TAMs with macrophage populations derived from other organs or tissue sites mainly reflect tissue differences rather than TAM-specific gene expression. As a consequence, we strongly propose to study TAMs in the context of their healthy tissue counterparts when searching for truly TAM-related changes in gene expression and functions. Clearly, this can be easier achieved in murine model systems compared to human cancer samples where healthy tissue from the same organ is often not accessible. More recently, Cassetta *et al*. reported on a 37-gene TAM signature derived from four breast cancer patients [17]. This signature was mainly enriched in the Her2 breast cancer subtype or the 'Claudin-low' molecular subtype as defined by the PAM50 classification [37]. Comparable to our results, this TAM signature could also be linked to worse outcome prediction of disease, albeit not specified for a particular breast cancer subtype which might be of importance for the development of new diagnostic and therapeutic strategies.

Indeed, another important finding of our study is the observation that only TAM-specific signatures derived from the KEP model were predictive for outcome in ILC patients. Although the two breast cancer models shared tumor-associated changes, such as the upregulation of genes associated with regulation of immune cells, we also observed functionality differences between the two murine models, such as the cell cycle. Differences in functions between breast cancer TAM populations have been previously described [38,39]. For instance, breast cancer TAM populations in different tumor models have been shown to differ in migratory behaviour and their ability to uptake fluorescent dextran [40]. Similarly, macrophage function can differ with varying oxygen levels across different tumor models [41,42]. Moreover, in the *MMTV-PyMT* mouse model both MTMs and TAMs are found in the mammary tumors, but only TAMs play a role in tumor progression [43,44]. Collectively, our findings show that the tumor subtype affects the phenotype of TAMs inducing a unique TAM signature in the two models.

While concerns have been raised about the validity of murine cancer models [45], we demonstrate here that a carefully designed cancer model, such as the KEP model can directly lead to clinically translatable results – here the generation of outcome prediction signatures based on TAM transcriptomes. For example, these signatures or marker genes (derived from such signatures) could now be tested in prospective clinical trials to assess their performance on outcome prediction. In this context, it is important to stress that only the KEP-TAM-derived, but not the NeuT-TAM-based gene signatures were informative for the ILC patient cohorts, further illustrating the requirement for murine tumor models that match with the patient tumor subtype. Such models are then ideally suited to address further questions concerning the role of the myeloid cell compartment within the TME [46].

While we could successfully translate population level information derived from the KEP model to a clinical question –namely outcome prediction–, other questions might need higher resolution analysis as it can be provided by single-cell -omics technologies [47]. Such a question in our study is the assessment of the underlying heterogeneity in the MTMs (PRE-KEP model). It is very likely that although these cells were found to be transcriptionally very similar to MTMs at the bulk population level, substructure analysis might reveal concealed homogeneous subsets with distinct transcriptomic profiles that follow a spectrum ranging from those of MTMs to KEP-TAMs. In this light, single-cell RNA-seq data from less than a hundred macrophages derived from 11 patients were described in an initial study [48] and a more recent study profiled more than 45,000 $CD45^+$ cells from 8 patients also including macrophages [23]. While particularly the second study highlighted the enormous heterogeneity of the immune cell compartment in breast cancer corroborating previous findings [11,12], it is too early to link this rich information to patient outcome prediction. Clearly, further studies are required that link approaches as presented here with these exciting new single cell -omics technologies to evaluate their clinical potential for diagnosis, subclassification of disease or outcome prediction.

Materials and methods

Animals

The generation and characterization of *K14cre;Cdh1$^{F/F}$;Trp53$^{F/F}$* mice have been previously described in detail [24]. The mice were backcrossed onto the FVB/N background and genotype was confirmed by PCR [24,49]. *MMTV-NeuT* mice on a Balb/c background [25] were purchased from Charles River Laboratories (Calco, Italy) and were bred in house. Female *K14cre;Cdh1$^{F/F}$;Trp53$^{F/F}$ and MMTV-NeuT* mice were monitored twice every week for the onset of mammary tumor formation by caliper and palpation measurement starting at 2 or 4 months of age, respectively. Mice were kept in open cages with food and water provided *ad libitum* at a 12-hour light/dark cycle. Animal experiments were approved by the Animal Ethics Committee of the Netherlands Cancer Institute (Amsterdam, Netherlands) and performed in accordance with institutional, national and European guidelines for Animal Care and Use (CCD license: AVD3010020172688).

Macrophage isolation

Macrophages were isolated according to [50]. Briefly, mammary glands or mammary tumors (size±225mm^2), spleen and bone marrow were harvested from 4 month old *K14cre;Cdh1$^{F/F}$;Trp53$^{F/F}$* female mice containing early lesions, 6-8 months old tumor-bearing *K14cre;Cdh1$^{F/F}$;Trp53$^{F/F}$*, 4 month old tumor-bearing *MMTV-NeuT* female mice and age- and sex-matched FVB/N and Balb/c mice. Tumors and mammary glands were mechanically chopped with a McIlwain Tissue Chopper (Ted Pella, Inc, CA, USA) and were enzymatically digested for 1 hour at 37°C with 3 mg/ml collagenase type A (Roche) and 1.5 mg/ml porcine pancreatic trypsin (BD Biosciences) in serum-free DMEM medium. Digestion was stopped by the addition of DMEM supplemented with 8% FBS and the suspension was disaggregated through a 70 µm cell strainer. Spleens and bone marrow cells from tibiae and femora were harvested and disaggregated through a 70 µm cell strainer. Splenic suspensions were subsequently treated twice with NH_4Cl erythrocyte lysis buffer for 3 min at room temperature. All single-cell suspensions were stained for 20 min at 4°C in the dark with anti-mouse F4/80 (1:200; BM8; eBioscience) and anti-mouse CD11b (1:200; M1/70; eBioscience) in IMDM supplemented with 2% FBS, 0.5% beta-mercaptoethanol, 0.5mM EDTA, Pen/Strep. Cells were then washed and incubated with magnetic MicroBeads (Miltenyi Biotec) following the manufacturer's guidelines. Isolation of F4/80$^+$ cells from the CD11b$^+$-enriched fraction was performed on a BD FACS ARIA II sorter with Diva software (BD Biosciences). DAPI was added to select viable cells. Sorted macrophages were stored at -80°C in TRIzol (Invitrogen). Cell purity was determined on a FACSCalibur using CellQuestPro software (BD Biosciences) and data were analyzed using FlowJo software v9.9.

Immunohistochemistry

Immunohistochemical analysis was performed by the Animal Pathology facility at the Netherlands Cancer Institute. Briefly, formaline-fixed paraffine-embedded tissues were blocked with 4% BSA/5% normal goat serum in PBS and stained with anti-mouse F4/80 (1:300; Cl:A3-1; AbD Serotec) after antigen retrieval with 20 ug/

ml Proteinase K (Sigma-Aldrich) at 37°C for 20 min. Endogenous peroxidase activity was neutralized in 3% H_2O_2 in methanol for 20 min at room temperature. Slides were then incubated with biotinylated goat anti-rat secondary antibody (1:100; SouthernBiotech) followed by DAB detection. Samples were visualized with a BX43 upright microscope (Olympus) and images were acquired in brightfield using cellSens Entry software (Olympus) at 40X magnification.

Flow cytometry

Single-cell suspensions were stained with anti-mouse CD45 (1:200; 30-F11; BD Biosciences), anti-mouse CD45 (1:200; 30-F11; eBioscience), anti-mouse CD11b (1:400; M1/70; Biolegend), anti-mouse CD11b (1:200; M1/70; eBioscience), anti-mouse F4/80 (1:200; BM8; eBioscience), anti-mouse CD206 (1:100; MR5D3; AbD Serotec), anti-mouse Ly-6C (1:400; HK1.4; eBioscience), anti-mouse Ly-6G (1:200; 1A8; BD Biosciences), anti-mouse Ly-6G (1:200; 1A8; Biolegend) and anti-mouse MHC-II (1:200; M5/114.15.2; eBioscience) for 20 min at 4°C in the dark in PBS supplemented with 0.5% BSA. 7AAD (1:20; eBioscience) or Fixable Viability Dye (1:1000; eBioscience) or Fixable aqua dead cell dye (1:100, ThermoFisher Scientific) were added to exclude dead cells. For Ki67 detection in macrophages, cells were fixed and permeabilized with the Foxp3/transcription factor staining Buffer set kit (ThermoFisher Scientific) as manufacturer's recommendations, followed by incubation with Fc block (CD16/CD32 purified; 1:50; 2.4G2; BD Biosciences) and stained with Ki67 or anti-mouse IgG2a. Experiments were performed using a LSRII flow cytometer (BD Biosciences) and data analysis were performed using FlowJo software v9.9.

Library preparation

Total RNA was extracted using the RNeasy Mini and Micro Kits (Qiagen). RNA (10 ng) was converted into cDNA libraries using the Ovation RNA-Seq system V2 and Encore Rapid library systems protocols (NuGEN) and samples were sequenced on a HiSeq 1500 system (Illumina).

Standard bioinformatic analysis

Publicly available datasets [16,28–31] were trimmed using fastx trimmer (*-l 50 -i Sample.fastq -o Sample_trim50.fastq*) to 50 bp reads to match our experimental settings. Our and the pre-processed publicly available data were aligned against the murine mm10 reference genome using TopHat2 (v2.0.11) default parameters [51]. The breast cancer datasets are available under GSE126268. Altogether three different datasets were composed; one containing only our two breast cancer models, one including our dataset and further available tissue macrophage datasets and another including our dataset and other tissue macrophage and immune cell types. The aligned reads were then imported into Partek Genomics Suite v6.6 (PGS) separately to deduct gene and transcript information before performing normalization using the DESeq2 package [52] in R (v3.0.2). Normalized read counts were floored to a value of at least 1 after batch correction. Finally, the datasets were filtered to a minimum value of 10 counts per group. The 1000 genes with the highest variance and DE gene calculations were performed utilizing a one-way ANOVA model in PGS. Genes with FC ≥ 2 and FDR ≤ 0.05 were defined as differentially expressed and were

visualized in volcano plots and FC/FC plots using SigmaPlot (v12.0) (Systat Software) and correlation plots. For more detailed analysis, the ANOVA model was filtered based on the respective gene lists [53]. TAM-specific surface marker expression was visualized in a heatmap using Mayday [54].

Comparative and biological function-related bioinformatic analysis
Global similarity comparisons between macrophage populations were performed by correlation analysis based on Pearson correlation coefficients (Pearson correlation ≥ 0.977) using BioLayout Express3D [55]. The correlation network was visualized in Cytoscape (http://www.cytoscape.org/). The structure of our breast cancer dataset was visualized utilizing PCA on all expressed genes. HC and PCCM were performed on the 1000 genes with the highest variance within the dataset using default settings in PGS. To link DE genes to known biological functions, GOEA was applied on DE gene sets extracted from FC/FC plots. Subsequently, Cytoscape was used to visualize GOEA results in a global view using the plug-ins BiNGO [56], EnrichmentMap[57] and Word Cloud[58].

CoCena²
To define differences and similarities in transcript expression patterns among the different groups, CoCena² (Construction of co-expression Network Analysis - automated) was performed based on Pearson correlation. Either all 15,425 present genes or the union of DE genes (2,123 genes) from the three comparisons KEP-TAMs versus MTMs from the KEP model, NeuT-TAMs versus MTMs from the NeuT model and KEP-TAMs versus MTMs from the PRE-KEP model were used as the input. Pearson correlation was performed using the R package Hmisc (v4.1-1). To increase data quality, only significant ($p<0.05$) correlation values were kept. A Pearson correlation coefficients cutoff of 0.878 (all present genes; 7,610 nodes and 310,789 edges) and of 0.87 (union DE genes; 1,992 nodes and 52,392 edges) was chosen to construct scale-free networks. The nodes were colored based on the Group Fold Change (GFC), the mean of each condition versus overall mean for each gene respectively, for each group separately. Unbiased clustering was performed using the "label propagation" algorithm in igraph (v1.2.1) and was repeated 1000 times. Genes assigned to more than 5 different clusters during the iterations got no cluster assignment. The mean GFC expression for each cluster and condition were visualized in the Cluster/Condition heatmap. Clusters smaller than 10 genes were not shown.

I-GIN (Intraclusteral Gene Interaction Network)
To further investigate condition-specific clusters (KEP and NeuT model shared signatures: turquoise [289 genes], NeuT-specific signatures: magenta [236 genes] and KEP-specific signatures: blue [255 genes]), an I-GIN was constructed based on the CoCena² results To enhance the structure and information access of the respective networks, hub genes were identified for each network separately. A gene was defined as hub gene, having a mean correlation greater or equal 75% of the connected edges. Maximal the top 25 most correlated and the two highest correlated edges with other hubs edges were visualized. All edges were classified as either already known or unknown via STRING database v1.20.0. Genes having

more than 5 known connections were additionally defined and labeled as hubs. All known interactions to hubs were kept and the resulting network nodes were sized according to their degree of connectivity in the resulting network. All edges in the network were colored grey and only known interactions were colored red. Hub genes were colored based on their property being regulating (purple) or being regulated (blue) by another gene. This information was calculated using Bayesian Network Analysis.

Bayesian Network Analysis

Bayesian Network Analysis is a probabilistic model that uses statistical dependencies and independencies between features to infer and describe their causal relations within the network. In this study, Bayesian Network Analysis was used to calculate the causal relationship of each gene pair within the cluster of interest defined by CoCena[2], providing additional information about the direction of regulation between two connected nodes within the I-GIN network. Bayesian Network Analysis extracted information from the turquoise, the blue and the magenta clusters and a greedy-search hill-climbing algorithm from the R-package "bnlearn" v4.4 [59] was used to create a network that best fits the observed data and represents the conditional dependencies and independencies between the genes within the cluster of interest. The network structure was then used to determine the regulatory status of each gene, classifying it as receiving if its number of parent nodes exceeded its number of children or as regulating if its number of children exceeded its number of parents. Genes were color-coded with respect to their regulatory status. We classified genes as "hot spots" with high regulatory potential, if their children-to-parent ratio (CP-ratio) exceeded the value 5.

Identification of TAM core signatures

Core signatures for breast cancer TAMs, KEP-TAMs, NeuT-TAMs were defined by overlapping CoCena[2] clusters and the respective DE genes. The breast cancer TAM core signatures are the intersection between the turquoise cluster and the common upregulated genes between KEP-TAMs versus MTMs (KEP model) and NeuT-TAMs versus MTMs (NeuT model). The KEP-TAM core signatures are the intersection between the blue cluster and the upregulated genes between KEP-TAMs versus MTMs (KEP model) and the NeuT-TAMs core signatures are the intersection between the magenta cluster and the upregulated genes between NeuT-TAMs versus MTMs (NeuT model). Subsequently, the union of the core signatures was visualized in a HC map using PGS.

CIBERSORT deconvolution analysis

CIBERSORT [34] was employed to characterize the relative contribution of immune cell populations to the TME of ILC patients. The normalized gene expression table of the TCGA ILC cohort was utilized as input mixture file and the published immune cell signatures "LM22" was used to compute the relative immune cell populations within bulk ILC samples (1,000 permutations). For custom signature generation by CIBERSORT, a gene expression matrix containing KEP-TAM and NeuT-TAM data was used as input.

TAM enrichment analysis

Bulk RNA-sequenced ILC TCGA specimens [27] were accessed through the Genomic Data Commons (https://gdc.cancer.gov/; phs000178.v9.p8) and were aligned against the human hg19 reference genome using TopHat2 (v2.0.11) default parameters. The data were normalized with DESeq2 in R (v3.0.2) and floored to a value of at least 1. Access to bulk ILC microarray specimens of the METABRIC cohort [26] was granted through the EGA depository (EGAD00010000162). The dataset was imported into PGS, quantile-normalized following log2 transformation of absolute expression values and subsequently filtered for probe sets exerting the highest variance. Genes were defined as expressed if the maximum value over all group means utilizing the classification in [27] was higher than 10 (TCGA) or 6.5 (log2 transformed; METABRIC). Before being able to ask whether the KEP-TAM or the NeuT-TAM signatures are enriched in the human TCGA or METABRIC datasets, the signatures were translated into human orthologues using the BioMart package [60] v2.36.1. The signature enrichment analysis for the human TCGA and METABRIC datasets was calculated using GSVA (v1.28.0) using the z-score method [61]. Enrichment analysis were performed for the KEP-TAM core signatures, NeuT-TAM core signatures, KEP-TAMs versus splenic macrophage core signatures (intersection of the blue cluster and KEP-TAM upregulated genes comparing KEP-TAMs versus splenic macrophages) and random signatures. Random gene signatures were generated by sampling a total of 450 genes from the union of signatures (breast cancer TAMs, KEP-TAMs and NeuT-TAMs) and randomly assigning them to three groups, each holding 150 genes. For each patient and each combination of dataset (TCGA and METABRIC) and signature, an enrichment score was calculated. The tool Cutoff Finder [62] was used to define the optimal enrichment score cutoff where a patient shows an enrichment of the respective signatures.

Kaplan Meier survival analysis

Kaplan-Meier survival analysis was performed utilizing the survival package in R (v3.0.2).

Acknowledgments

We thank H-S. Sow for technical assistance. We would like to acknowledge the flow cytometry facility, the animal facility and the animal pathology facility at the Netherlands Cancer Institute. Research in the KEdV lab is supported by the European Union (FP7 MCA-ITN 317445 TIMCC), the Dutch Cancer Society (NKI10623), the European Research Council (ERC consolidator award INFLAMET 615300) and Oncode. JLS is supported by the DFG (EXC 2151/1), the Helmholtz-funded project Sparse2Big, and the European Union (H2020, No 733100: SYSCID, A systems medicine approach to chronic inflammatory diseases).

Authors contributions

JLS, KEdV and TU designed the study. ST, CS and CSH performed experiments. ST, CS, LS, MO, KK and TU performed analysis. TSK wrote the manuscript with input from all authors.

Competing interests

The authors declare no competing interests.

References

1. Chen, D. S. & Mellman, I. Oncology Meets Immunology: The Cancer-Immunity Cycle. *Immunity* **39,** 1–10 (2013).
2. Shalapour, S. & Karin, M. Immunity, inflammation, and cancer: an eternal fight between good and evil. *J. Clin. Invest.* **125,** 3347–55 (2015).
3. The Nobel Prize in Physiology or Medicine 2018. Available at: https://www.nobelprize.org/prizes/medicine/2018/summary/. (Accessed: 17th October 2018)
4. Ruffell, B. *et al.* Leukocyte composition of human breast cancer. *Proc. Natl. Acad. Sci. U. S. A.* **109,** 2796–801 (2012).
5. Noy, R. & Pollard, J. W. Tumor-Associated Macrophages: From Mechanisms to Therapy. *Immunity* **41,** 49–61 (2014).
6. Quatromoni, J. G. & Eruslanov, E. Tumor-associated macrophages: function, phenotype, and link to prognosis in human lung cancer. *Am. J. Transl. Res.* **4,** 376–89 (2012).
7. Zhao, X. *et al.* Prognostic significance of tumor-associated macrophages in breast cancer: a meta-analysis of the literature. *Oncotarget* **8,** 30576–30586 (2017).
8. Hoadley, K. A. *et al.* Cell-of-Origin Patterns Dominate the Molecular Classification of 10,000 Tumors from 33 Types of Cancer. *Cell* **173,** 291–304.e6 (2018).
9. Thorsson, V. *et al.* The Immune Landscape of Cancer. *Immunity* **48,** 812–830.e14 (2018).
10. Gentles, A. J. *et al.* The prognostic landscape of genes and infiltrating immune cells across human cancers. *Nat. Med.* **21,** 938–945 (2015).
11. Iqbal, J. *et al.* Molecular signatures to improve diagnosis in peripheral T-cell lymphoma and prognostication in angioimmunoblastic T-cell lymphoma. *Blood* **115,** 1026–36 (2010).
12. Johdi, N. A., Ait-Tahar, K., Sagap, I. & Jamal, R. Molecular Signatures of Human Regulatory T Cells in Colorectal Cancer and Polyps. *Front. Immunol.* **8,** 620 (2017).
13. Lyons, Y. A., Wu, S. Y., Overwijk, W. W., Baggerly, K. A. & Sood, A. K. Immune cell profiling in cancer: molecular approaches to cell-specific identification. *NPJ Precis. Oncol.* **1,** 26 (2017).
14. Gosselin, D. *et al.* Environment Drives Selection and Function of Enhancers Controlling Tissue-Specific Macrophage Identities. *Cell* **159,** 1327–1340 (2014).
15. Mass, E. *et al.* Specification of tissue-resident macrophages during organogenesis. *Science* **353,** aaf4238-aaf4238 (2016).
16. Lavin, Y. *et al.* Tissue-Resident Macrophage Enhancer Landscapes Are Shaped by the Local Microenvironment. *Cell* **159,** 1312–1326 (2014).
17. Cassetta, L. *et al.* Human Tumor-Associated Macrophage and Monocyte Transcriptional Landscapes Reveal Cancer-Specific Reprogramming, Biomarkers, and Therapeutic Targets. *Cancer Cell* (2019). doi:10.1016/j.ccell.2019.02.009
18. Regev, A. *et al.* The Human Cell Atlas. *Elife* **6,** (2017).
19. Lavin, Y. *et al.* Innate Immune Landscape in Early Lung Adenocarcinoma by Paired Single-Cell Analyses. *Cell* **169,** 750–765.e17 (2017).
20. Lambrechts, D. *et al.* Phenotype molding of stromal cells in the lung tumor microenvironment. *Nat. Med.* **24,** 1277–1289 (2018).
21. Tirosh, I. *et al.* Dissecting the multicellular ecosystem of metastatic melanoma by single-cell RNA-seq. *Science (80-.).* **352,** 189–196 (2016).
22. Savas, P. *et al.* Single-cell profiling of breast cancer T cells reveals a tissue-resident memory subset associated with improved prognosis. *Nat. Med.* **24,** 986–993 (2018).
23. Azizi, E. *et al.* Single-Cell Map of Diverse Immune Phenotypes in the Breast Tumor Microenvironment. *Cell* **174,** 1293–1308.e36 (2018).
24. Derksen, P. W. B. *et al.* Somatic inactivation of E-cadherin and p53 in mice leads to metastatic lobular mammary carcinoma through induction of anoikis resistance and angiogenesis. *Cancer Cell* **10,** 437–49 (2006).

25. Boggio, K. *et al.* Interleukin 12-mediated prevention of spontaneous mammary adenocarcinomas in two lines of Her-2/neu transgenic mice. *J. Exp. Med.* **188,** 589–96 (1998).
26. Curtis, C. *et al.* The genomic and transcriptomic architecture of 2,000 breast tumours reveals novel subgroups. *Nature* **486,** 346–52 (2012).
27. Ciriello, G. *et al.* Comprehensive Molecular Portraits of Invasive Lobular Breast Cancer. *Cell* **163,** 506–19 (2015).
28. Squadrito, M. L. *et al.* miR-511-3p modulates genetic programs of tumor-associated macrophages. *Cell Rep.* **1,** 141–54 (2012).
29. Choi, H. *et al.* Transcriptome analysis of individual stromal cell populations identifies stroma-tumor crosstalk in mouse lung cancer model. *Cell Rep.* **10,** 1187–201 (2015).
30. Lu, L.-F. *et al.* A Single miRNA-mRNA Interaction Affects the Immune Response in a Context- and Cell-Type-Specific Manner. *Immunity* **43,** 52–64 (2015).
31. Thomas, G. D. *et al.* The biology of nematode- and IL4Rα-dependent murine macrophage polarization in vivo as defined by RNA-Seq and targeted lipidomics. *Blood* **120,** e93–e104 (2012).
32. Biswas, S. K. *et al.* A distinct and unique transcriptional program expressed by tumor-associated macrophages (defective NF-kappaB and enhanced IRF-3/STAT1 activation). *Blood* **107,** 2112–22 (2006).
33. Ojalvo, L. S., King, W., Cox, D. & Pollard, J. W. High-density gene expression analysis of tumor-associated macrophages from mouse mammary tumors. *Am. J. Pathol.* **174,** 1048–64 (2009).
34. Newman, A. M. *et al.* Robust enumeration of cell subsets from tissue expression profiles. *Nat. Methods* **12,** 453–7 (2015).
35. Aras, S. & Zaidi, M. R. TAMeless traitors: macrophages in cancer progression and metastasis. *Br. J. Cancer* **117,** 1583–1591 (2017).
36. Poh, A. R. & Ernst, M. Targeting Macrophages in Cancer: From Bench to Bedside. *Front. Oncol.* **8,** 49 (2018).
37. Parker, J. S. *et al.* Supervised risk predictor of breast cancer based on intrinsic subtypes. *J. Clin. Oncol.* **27,** 1160–7 (2009).
38. Qian, B.-Z. & Pollard, J. W. Macrophage diversity enhances tumor progression and metastasis. *Cell* **141,** 39–51 (2010).
39. Kim, I. S. & Zhang, X. H.-F. One microenvironment does not fit all: heterogeneity beyond cancer cells. *Cancer Metastasis Rev.* **35,** 601–629 (2016).
40. Egeblad, M. *et al.* Visualizing stromal cell dynamics in different tumor microenvironments by spinning disk confocal microscopy. *Dis. Model. Mech.* **1,** 155–167 (2008).
41. Movahedi, K. *et al.* Different tumor microenvironments contain functionally distinct subsets of macrophages derived from Ly6C(high) monocytes. *Cancer Res.* **70,** 5728–39 (2010).
42. Casazza, A. *et al.* Impeding macrophage entry into hypoxic tumor areas by Sema3A/Nrp1 signaling blockade inhibits angiogenesis and restores antitumor immunity. *Cancer Cell* **24,** 695–709 (2013).
43. Franklin, R. A. *et al.* The cellular and molecular origin of tumor-associated macrophages. *Science (80-.).* **344,** 921–925 (2014).
44. Tymoszuk, P. *et al.* In situ proliferation contributes to accumulation of tumor-associated macrophages in spontaneous mammary tumors. *Eur. J. Immunol.* **44,** 2247–2262 (2014).
45. Mak, I. W., Evaniew, N. & Ghert, M. Lost in translation: animal models and clinical trials in cancer treatment. *Am. J. Transl. Res.* **6,** 114–8 (2014).
46. Salvagno, C. *et al.* Therapeutic targeting of macrophages enhances chemotherapy efficacy by unleashing type I interferon response. *Nat. Cell Biol.* **21,** 511–521 (2019).
47. Papalexi, E. & Satija, R. Single-cell RNA sequencing to explore immune cell heterogeneity. *Nat. Rev. Immunol.* **18,** 35–45 (2017).
48. Ferreri, A. J. M., Illerhaus, G., Zucca, E., Cavalli, F. & Group, on behalf of the I. E. L. S. Flows and flaws in primary central nervous system lymphoma. *Nat. Rev. Clin. Oncol.* **7,** 1–2 (2010).
49. Coffelt, S. B. *et al.* IL-17-producing γδ T cells and neutrophils conspire to promote breast cancer metastasis. *Nature* **522,** 345–348 (2015).

50. Salvagno, C. & de Visser, K. E. Purification of Immune Cell Populations from Freshly Isolated Murine Tumors and Organs by Consecutive Magnetic Cell Sorting and Multi-parameter Flow Cytometry-Based Sorting. *Methods Mol. Biol.* **1458,** 125–35 (2016).
51. Kim, D. *et al.* TopHat2: accurate alignment of transcriptomes in the presence of insertions, deletions and gene fusions. *Genome Biol.* **14,** R36 (2013).
52. Love, M. I., Huber, W. & Anders, S. Moderated estimation of fold change and dispersion for RNA-seq data with DESeq2. *Genome Biol.* **15,** 550 (2014).
53. Fulton, D. L. *et al.* TFCat: the curated catalog of mouse and human transcription factors. *Genome Biol.* **10,** R29 (2009).
54. Battke, F., Symons, S. & Nieselt, K. Mayday - integrative analytics for expression data. *BMC Bioinformatics* **11,** 121 (2010).
55. Theocharidis, A., van Dongen, S., Enright, A. J. & Freeman, T. C. Network visualization and analysis of gene expression data using BioLayout Express(3D). *Nat. Protoc.* **4,** 1535–50 (2009).
56. Maere, S., Heymans, K. & Kuiper, M. BiNGO: a Cytoscape plugin to assess overrepresentation of gene ontology categories in biological networks. *Bioinformatics* **21,** 3448–9 (2005).
57. Merico, D., Isserlin, R., Stueker, O., Emili, A. & Bader, G. D. Enrichment map: a network-based method for gene-set enrichment visualization and interpretation. *PLoS One* **5,** e13984 (2010).
58. Oesper, L., Merico, D., Isserlin, R. & Bader, G. D. WordCloud: a Cytoscape plugin to create a visual semantic summary of networks. *Source Code Biol. Med.* **6,** 7 (2011).
59. Scutari, M. Learning Bayesian Networks with thebnlearnRPackage. *J. Stat. Softw.* **35,** (2010).
60. Durinck, S., Spellman, P. T., Birney, E. & Huber, W. Mapping identifiers for the integration of genomic datasets with the R/Bioconductor package biomaRt. *Nat. Protoc.* **4,** 1184–1191 (2009).
61. Hänzelmann, S., Castelo, R. & Guinney, J. GSVA: gene set variation analysis for microarray and RNA-seq data. *BMC Bioinformatics* **14,** 7 (2013).
62. Budczies, J. *et al.* Cutoff Finder: a comprehensive and straightforward Web application enabling rapid biomarker cutoff optimization. *PLoS One* **7,** e51862 (2012).

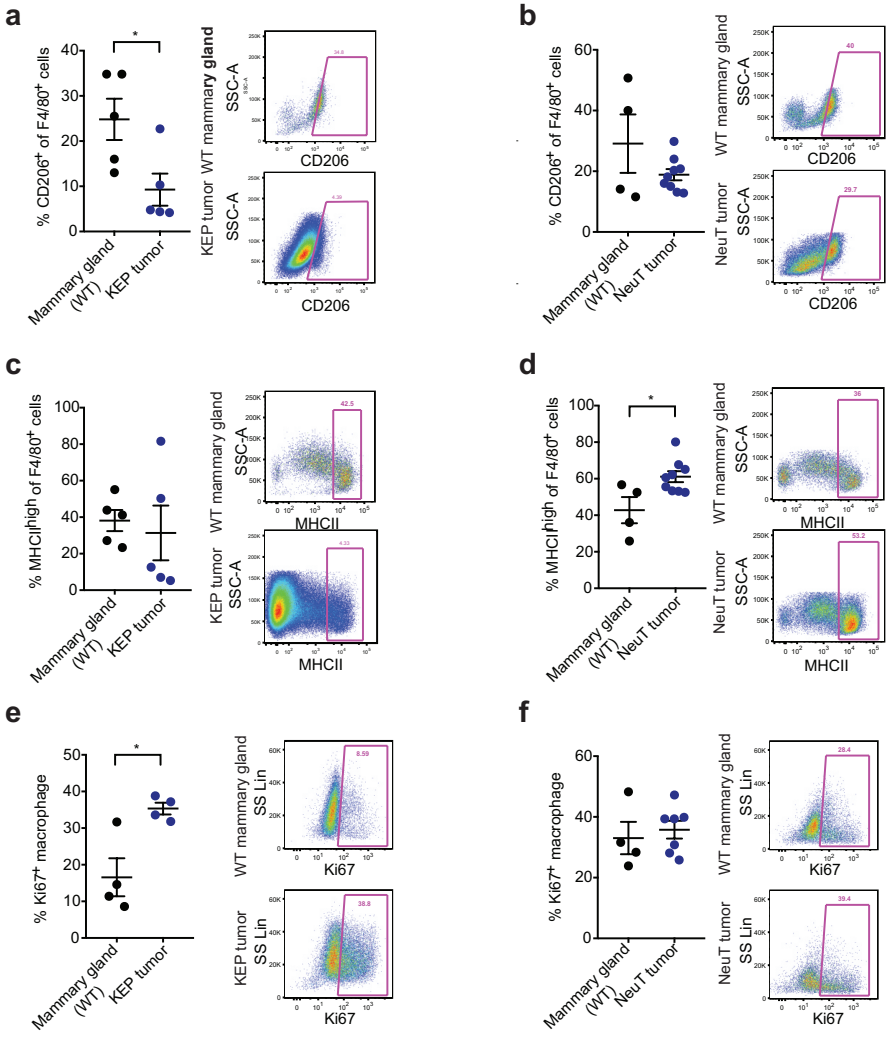

Supplementary Fig. 1 | Related to Fig. 1. TAMs in K14cre;Cdh1$^{F/F}$;Trp53$^{F/F}$ mammary tumors express low levels of CD206 and have a proliferative phenotype compared to TAMs from the MMTV-NeuT model. (a-b) Percentage of CD206^{+} macrophages in KEP tumors and WT FVB mammary glands (a) or NeuT tumors and WT Balb/c mammary glands (b) as determined by flow cytometry. Representative dot plots are shown. The gating was based on fluorescence-minus-one sample for CD206. (c-d) Percentage of MHC-II^{+} macrophages in KEP tumors and WT FVB mammary glands (c) or NeuT tumors and WT Balb/c mammary glands (d) as determined by flow cytometry. Representative dot plots are shown. (e-f) Percentage of Ki67^{+} macrophages in KEP tumors and WT FVB mammary glands (e) or in NeuT mammary tumor and WT Balb/c mammary glands (f) as determined by flow cytometry. Dot plots were gated on CD11b^{+}F4/80^{+} macrophages. Representative dot plots are shown. Data are mean values ± SEM from n=3 animals per group and were analyzed with Mann-Whitney test, *p < 0.05.

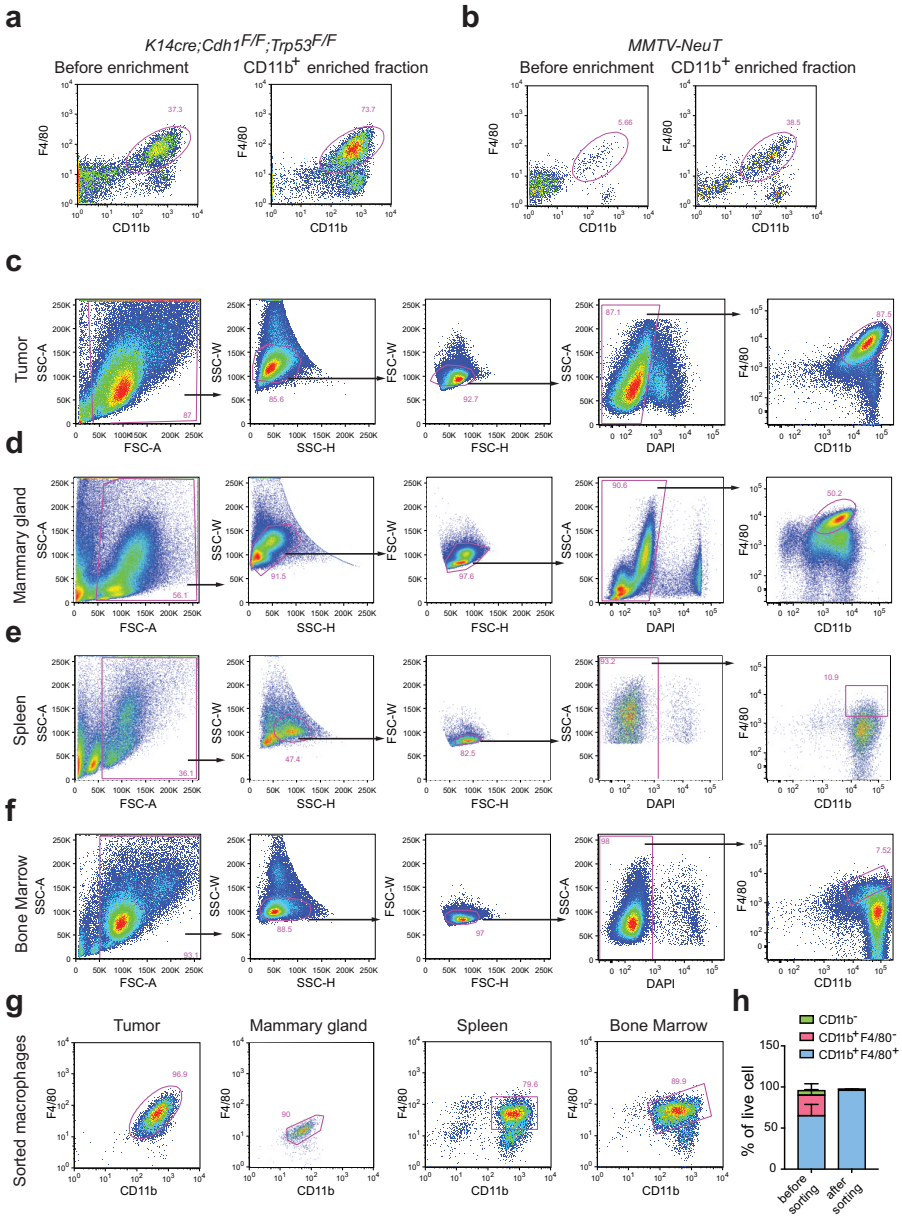

Supplementary Fig. 2 | Isolation procedure of CD11b$^+$F4/80$^+$ macrophages from mammary tumor, mammary gland, spleen and bone marrow by magnetic and fluorescence-activated cell sorting. (a-b) Representative dot plots of KEP (a) and NeuT (b) mammary tumors showing the CD11b$^+$F4/80$^+$ population before and after pre-enrichment by magnetic-activated cell sorting for CD11b$^+$ cells. (c-f) Representative dot plots illustrating the gating strategy for the isolation of CD11b$^+$F4/80$^+$ macrophages from KEP tumors (c), mammary gland (d), spleen (e) and bone marrow (f) by fluorescence-activated cell sorting after enrichment of CD11b$^+$ cells. (g) Dot plots showing the purity of the sorted macrophages in tumor, mammary gland, spleen and bone marrow of KEP mice. (h) Stacked bar plots showing the composition of KEP tumors in CD11b$^-$, CD11b$^+$F4/80$^-$ and CD11b$^+$F4/80$^+$ cells before and after macrophage sorting. Data are mean values ± SEM from 3 preps.

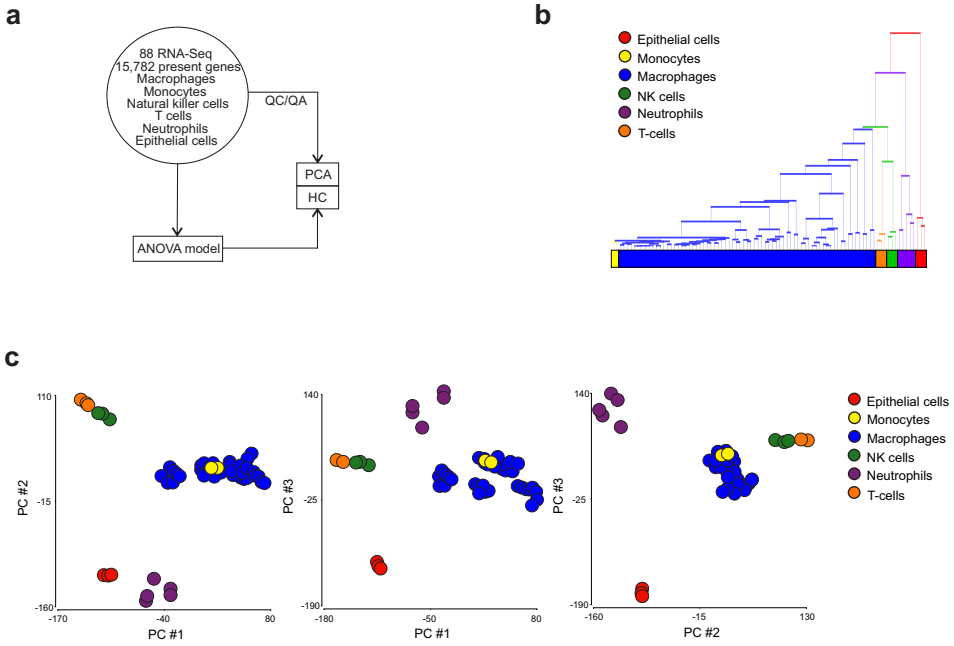

Supplementary Fig. 3 | Murine macrophages are distinguished from other immune cell populations by their transcriptome. (a) Schematic representation outlining bioinformatics workflow. (b) HC based on the 1,000 genes with the highest variance within the dataset. Macrophage transcriptomes derived from different organs (mammary gland, bone marrow, spleen, peritoneum, lung, brain, liver, large intestine and small intestine) and disease states (tumor, pre-lesion and helminth infection) were collectively named macrophages. (c) PCA using all present (15,782) genes with principle components (PC1-3) plotted in two-dimensional graphs.

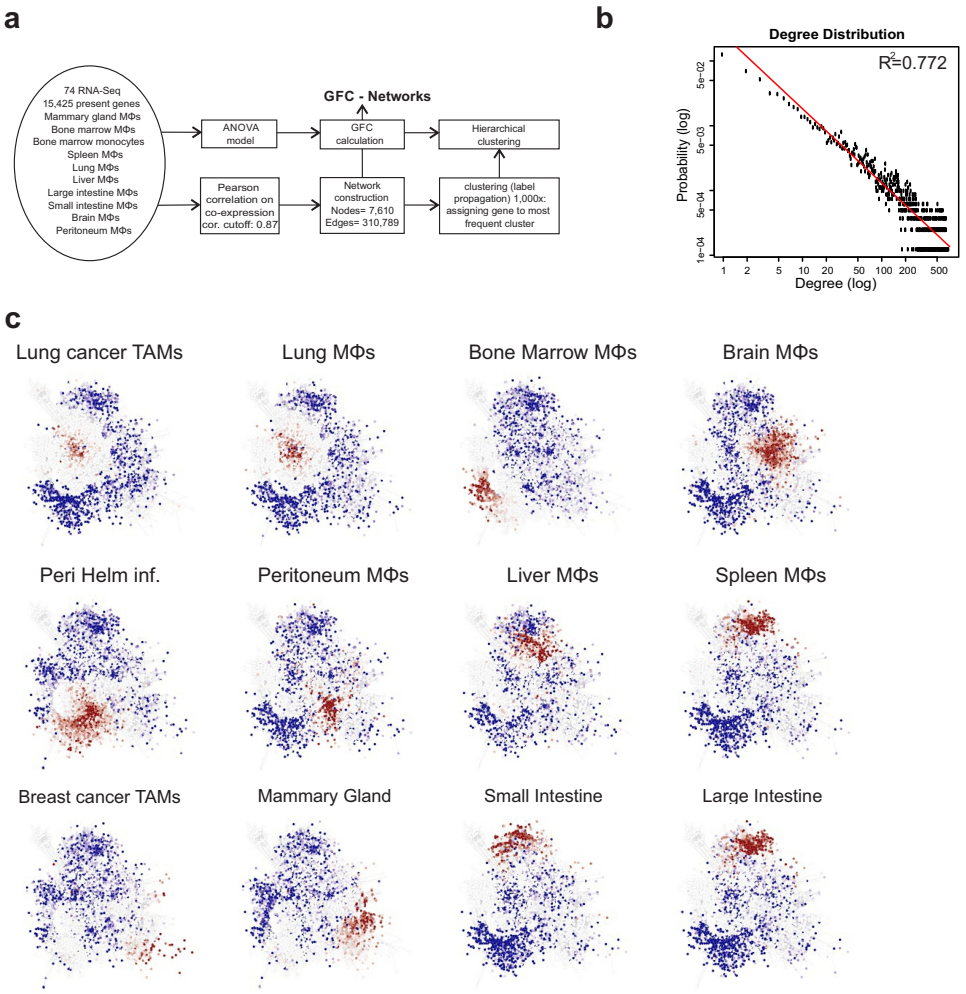

Supplementary Fig. 4 | Co-expression network analysis (CNA) of all present genes by CoCena². (a) Schematic representation depicting the bioinformatics workflow. (b) CoCena² logged network degree distribution with linear fitting. (c) Networks were colored according to Group Fold Changes (GFCs) for each condition, respectively (condition mean versus overall mean).

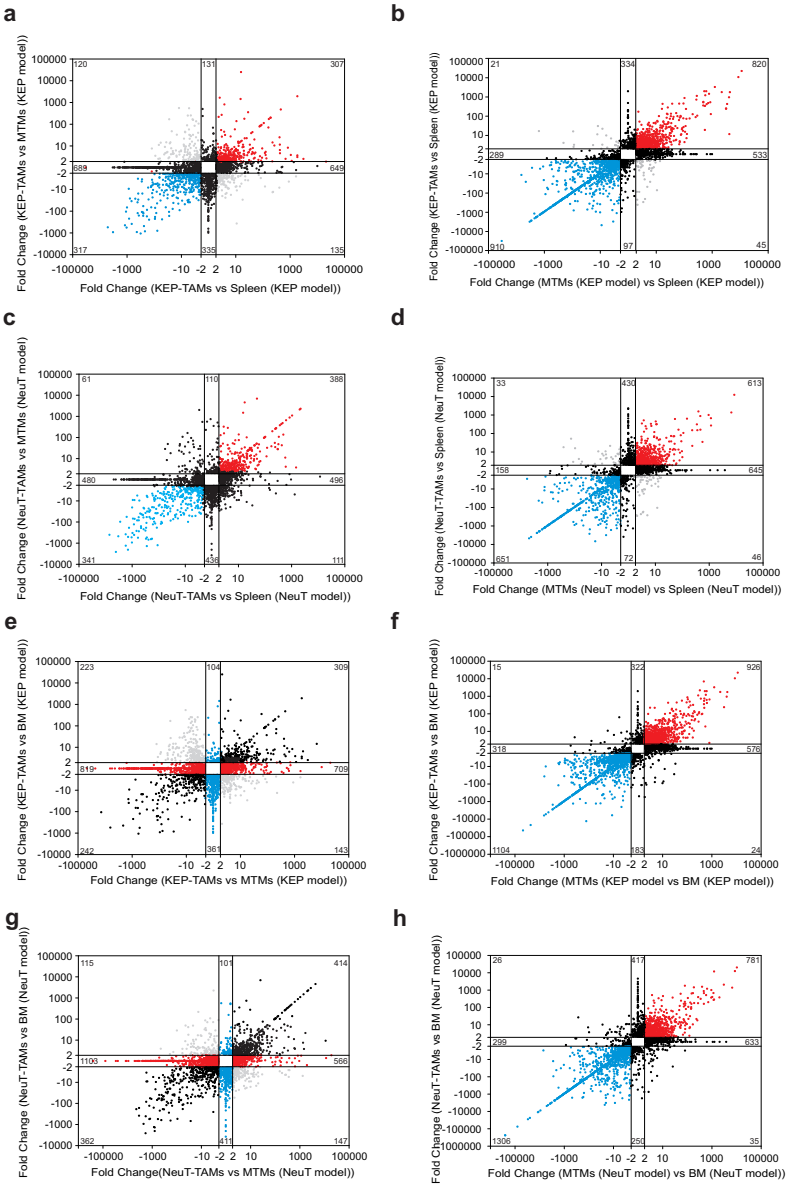

Supplementary Fig. 5 | Inter-tissue comparison leads to false interpretation of changes in TAMs. (a) FC/FC plot of the union of DE genes showing the fold change in expression of genes in KEP-TAMs compared to MTMs (KEP model) (y-axis) against KEP-TAMs compared to splenic macrophages (KEP model) (x-axis). (b) FC/FC plot of the union of DE genes showing the fold change in expression of genes in KEP-TAMs compared to splenic macrophages (KEP model) (y-axis) against MTMs (KEP model) compared to splenic macrophages (KEP model) (x-axis). (c) FC/FC plot of the union of DE genes showing the fold change in expression of genes in NeuT-TAMs compared to MTMs (NeuT model) (y-axis) against NeuT-TAMs compared to splenic macrophages (NeuT model) (x-axis). (d) FC/FC plot of the union of DE genes showing the fold change in expression of genes in NeuT-TAMs compared to splenic macrophages (NeuT model) (y-axis) against MTMs (NeuT model) compared to splenic macrophages (NeuT model) (x-axis). (e) FC/FC plot of the union of DE genes showing the fold change in expression of genes in

KEP-TAMs compared to bone marrow macrophages (KEP model) (y-axis) against KEP-TAMs compared to MTMs (KEP model) (x-axis). (f) FC/FC plot of the union of DE genes showing the fold change in expression of genes in KEP-TAMs compared to bone marrow macrophages (KEP model) (y-axis) against MTMs (KEP model) compared to bone marrow macrophages (KEP model) (x-axis). (g) FC/FC plot of the union of DE genes showing the fold change in expression of genes in NeuT-TAMs compared to bone marrow macrophages (NeuT model) (y-axis) against NeuT-TAMs compared to MTMs (NeuT model) (x-axis). (h) FC/FC plot of the union of DE genes showing the fold change in expression of genes in NeuT-TAMs compared to bone marrow macrophages (NeuT model) (y-axis) against MTMs (NeuT model) compared to bone marrow macrophages (NeuT model) (x-axis). Each dot represents one gene where red and blue dots indicate positive or negative fold change differences in both comparisons and grey dots correspond to opposite fold change differences across the axes.

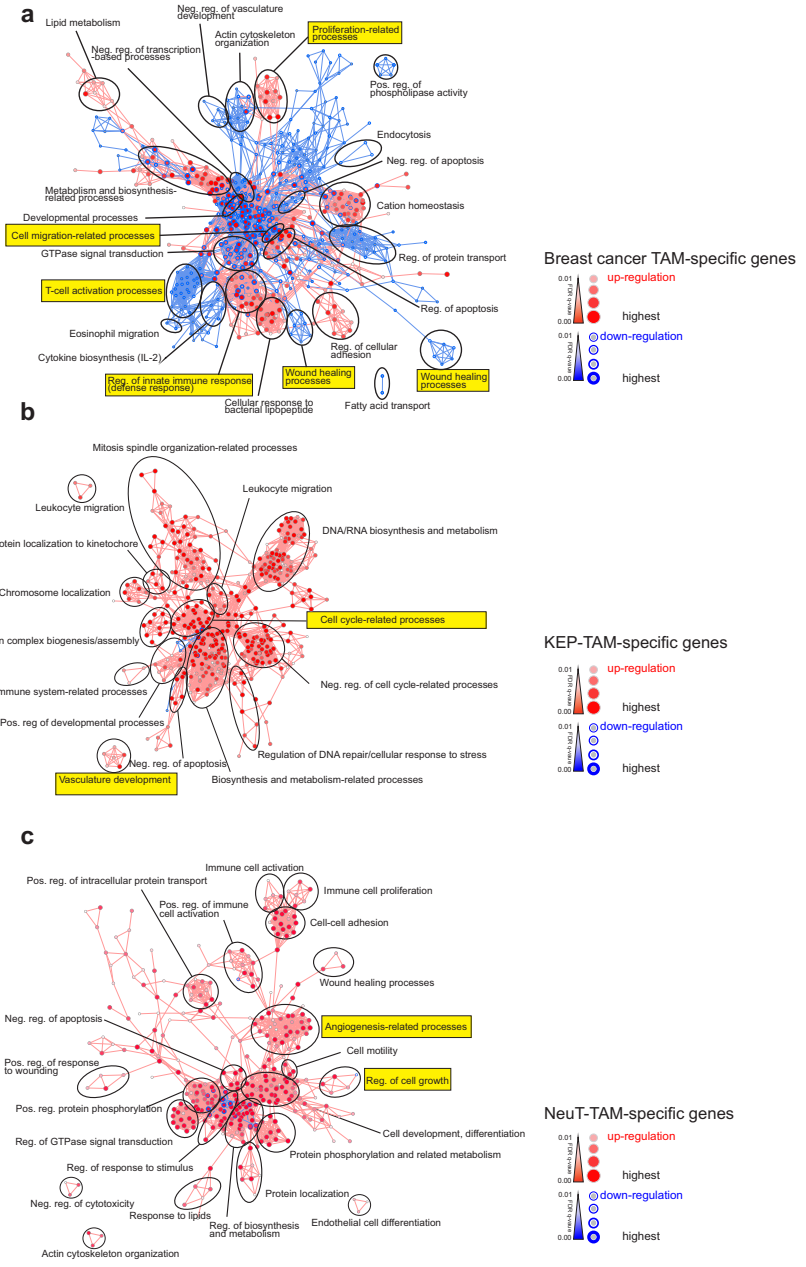

Supplementary Fig. 6 | GOEA of breast cancer TAM-, KEP-TAM- and NeuT-TAM-specific genes. (a-c) Network visualization of GOEA using BiNGO and EnrichmentMap based on model-specific DE genes derived from (a) breast cancer TAM-, (b) KEP-TAM- and (c) NeuT-TAM-specific genes. Node size and color (positively enriched GO terms) and node border width (negatively enriched GO terms) represent corresponding FDR-adjusted enrichment p-values (p-value: ≤0.05). Enriched gene ontology terms mentioned in the text are highlighted in yellow boxes.

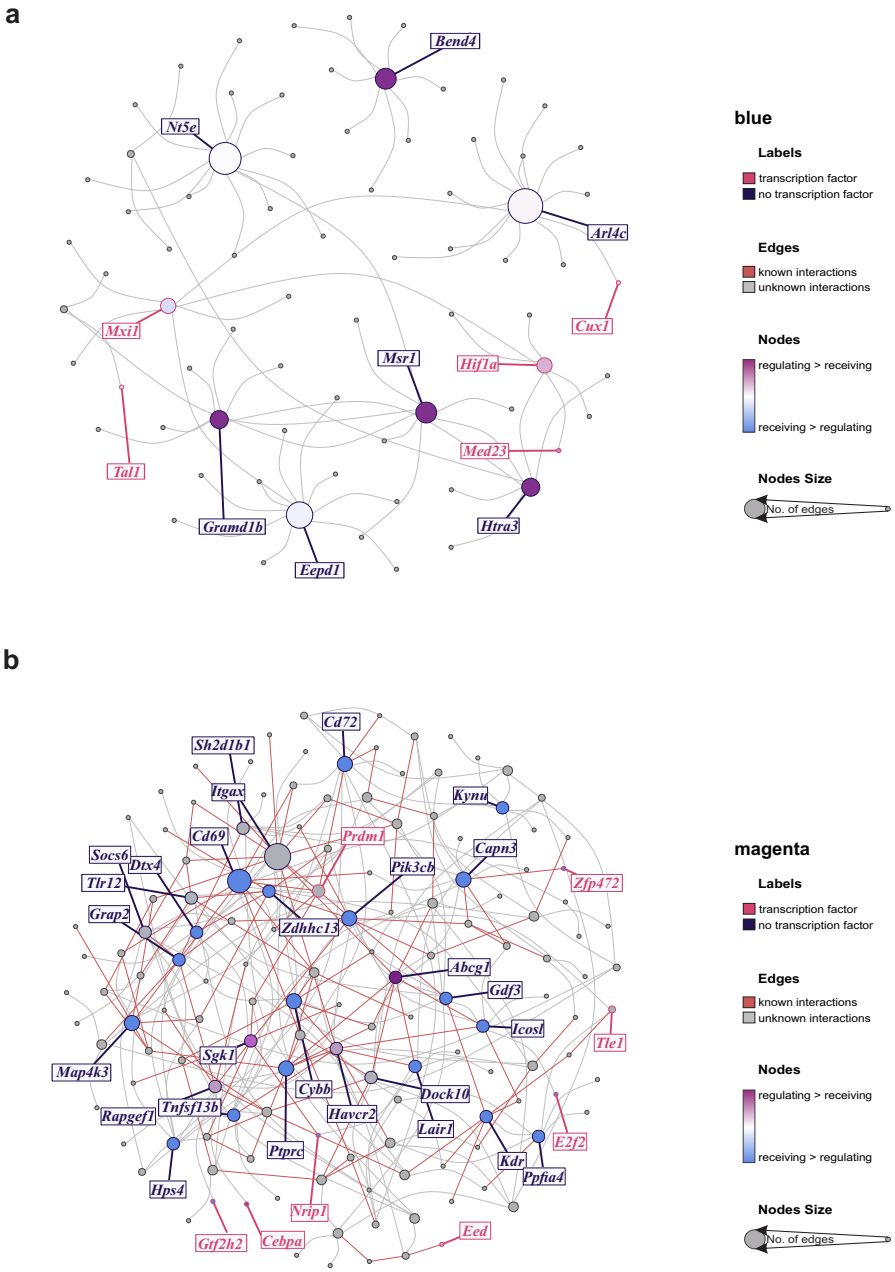

Supplementary Fig. 7 | I-GIN of KEP-TAM- and NeuT-TAM-specific genes. (a-b) I-GIN construction for KEP-TAM-specific (blue cluster) (a) and NeuT-specific (magenta cluster) (b) genes. Node coloring represents regulatory or receiving status obtained from a Bayesian approach and points out highly co-expressed genes and their known or proposed links to strongest correlated neighbors. Candidate genes mentioned in the text are highlighted in yellow boxes.

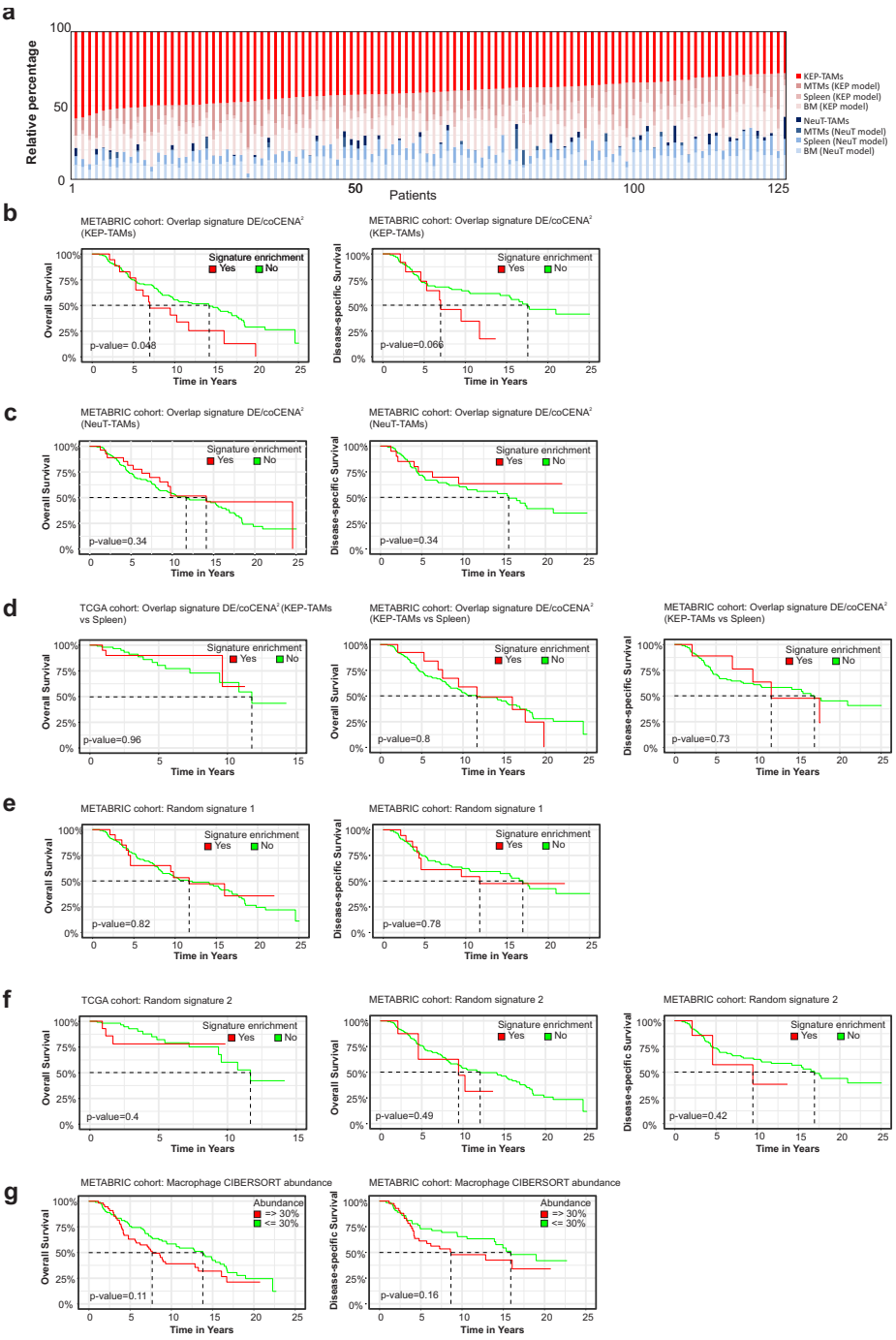

Supplementary Fig. 8 | Validation of Kaplan-Meier survival analysis of breast cancer model-specific signatures. (a) KEP-TAM, NeuT-TAM, splenic and bone marrow macrophage and MTM signatures from both models were computed using CIBERSORT and their relative abundance in the ILC specimens was calculated. (b) Kaplan-Meier overall (left) and disease-specific (right) survival analysis of METABRIC ILC patients (n=147). ILC specimens having a significant enrichment for KEP-TAMs signature are

visualized in red line and numbers. The rest ILC patients are visualized in green line and numbers. (c) Kaplan-Meier overall (left) and disease-specific (right) survival analysis of METABRIC ILC patients. ILC specimens having a significant enrichment for NeuT-TAMs signature are visualized in red line and numbers. The rest ILC patients are visualized in green line and numbers. (d) Kaplan-Meier overall (left and middle) and disease-specific (right) survival analysis of TCGA (left, n=125) and METABRIC (middle and right) ILC patients. ILC specimens having a significant enrichment for KEP-TAMs signature (using splenic macrophages from the KEP model as a control) are visualized in red line and numbers. The rest ILC patients are visualized in green line and numbers. (e) Kaplan-Meier overall (left) and disease-specific (right) survival analysis of METABRIC ILC patients. ILC specimens having a significant enrichment for a random signature are visualized in red line and numbers. The rest ILC patients are visualized in green line and numbers. (f) Kaplan-Meier overall (left and middle) and disease-specific (right) survival analysis of TCGA (left) and METABRIC (middle and right) ILC patients. ILC specimens having a significant enrichment for a random signature macrophage signature are visualized in red line and numbers. The rest ILC patients are visualized in green line and numbers. (g) Kaplan-Meier overall (left) and disease-specific (right) survival analysis of METABRIC ILC patients. ILC specimens having a significant enrichment for a CIBERSORT macrophage signature are visualized in red line and numbers. The rest ILC patients are visualized in green line and numbers. Z score above 2 marks significant enrichment of gene signatures.